spectrum of the black nail was different from that of the normal nail and ZnS. Thus, different chemical species of Zn seem to exist in the black nail.

With regard to the XAFS study of human nails, Katsukini et al. reported the findings of extended X-ray absorption fine structure (EXAFS) analysis of Zn in human nails [9]. They assumed that Zn coordinates with the nitrogen (N) and S contained in histidine and cysteine, which are the major amino acids of nail keratin. They also reported that the coordination numbers and bond lengths of N and S varied depending on the manifestation (clubbed nail, tuberculosis, and fibrosis). In our study, we observed a definite difference in the Zn K-edge XANES spectra between the black nail and the normal nail, and we inferred the presence of different chemical species in the black nail. Thus, element analysis by XRF and the chemical state analysis by XAFS of nails would be useful for the diagnosis of conditions of human nails.

Conclusion

The XRF and XAFS analyses were performed to assess the element composition and the chemical state of the discolored nails. XRF analysis revealed that the normal nail contained a higher concentration of S derived from nail keratin but a lower concentration of Ca and Zn. A part of the yellow nail showed considerably higher Ca content, and we therefore inferred that the yellow nail contains a good proportion of calcified matter. Compared to the other nail samples, the black nail contained a higher concentration of Ca and much higher concentration of Zn. The chemical state of Zn, as estimated by XAFS, in the yellow nail was similar to that in the normal nail. The Zn present in the black nail showed a slightly different chemical state, and therefore, we inferred the existence of different chemical species of Zn in the black nail.

Acknowledgements

The XAFS measurements were conducted after receiving approval of the Photon Factory Advisory Committee (Proposal No. 2010G022). This work was supported by a Grant-in-Aid for Challenging Exploratory Research No. 21659449, from the Ministry of Education, Culture, Sports, Science and Technology, Japan.

References

1) Cashman MW, Sloan SB. Nutrition and nail disease. Clin Dermatol 2010;28;420-425.
2) Shimizu H. Shimizu's Textbook of Dermatology, Hokkaido University Press, Sapporo, pp. 324-326.
3) Zuehlke RL, Taylor WB. Black nails with Proteus mirabilis. Arch Derm 1970;102:154-155.
4) Kamalam A, Ajithadass K, Sentamilselvi G, Thambiah AS. Paronychia and black discoloration of a thumb nail caused by Curvularia lunata. Mycopathologia 1992;118:83-84.
5) Maldonado F, Tazalaar HD, Wang CW, Ryu JH. Yellow nail syndrome: Analysis of 41 consecutive patients. Chest 2008;134:375-381.
6) Arroyo JF, Cohen ML. Improvement of yellow nail syndrome with oral zinc supplementation. Clin Exp Dermatol 1993;18:62-64.
7) van Sprang HA. Fundamental parameter methods in XRF spectroscopy. Adv X-ray Anal 2000;42:1-10.
8) Karita K, Takano T, Nakamura S, Haga N, Iwaya T. A search for calcium, magnesium and zinc levels in fingernails of 135 patients with osteogenesis imperfecta. J Trace Elem Med Biol 2001;15:36-39.
9) Katsukini M, Mavromati E, Pinakidou F, Paloura EC, Gioulekas D. Zn-K edge EXAFS study of human nails. J Phys: Conference Series 2009;190:012204.

(Received: November 10/
Accepted: December 18)

Corresponding author:
Motohiro Uo, Ph.,D.
Department of Biomedical Materials and Engineering, Graduate School of Dental Medicine, Hokkaido University
North 13, West 7, Kita-ku,
Sapporo 060-8586, Japan
Tel: +81-11-706-4251
e-mail: mail@m-uo.com

The Journal of Immunology

A Novel Active Mouse Model for Bullous Pemphigoid Targeting Humanized Pathogenic Antigen

Hideyuki Ujiie, Akihiko Shibaki, Wataru Nishie, Daisuke Sawamura, Gang Wang, Yasuki Tateishi, Qiang Li, Reine Moriuchi, Hongjiang Qiao, Hideki Nakamura, Masashi Akiyama and Hiroshi Shimizu

J. Immunol. 2010;184;2166-2174; originally published online Jan 20, 2010;
doi:10.4049/jimmunol.0903101
http://www.jimmunol.org/cgi/content/full/184/4/2166

The Journal of Immunology is published twice each month by The American Association of Immunologists, Inc., 9650 Rockville Pike, Bethesda, MD 20814-3994.

Print ISSN: 0022-1767 Online ISSN: 1550-6606.

A Novel Active Mouse Model for Bullous Pemphigoid Targeting Humanized Pathogenic Antigen

Hideyuki Ujiie, Akihiko Shibaki, Wataru Nishie, Daisuke Sawamura, Gang Wang, Yasuki Tateishi, Qiang Li, Reine Moriuchi, Hongjiang Qiao, Hideki Nakamura, Masashi Akiyama, and Hiroshi Shimizu

Bullous pemphigoid (BP), the most common autoimmune blistering disease, is caused by autoantibodies against type XVII collagen (COL17). To establish an active stable BP animal model that demonstrates the persistent inflammatory skin lesions initiated by the anti-human COL17 Abs, we used COL17-humanized (*COL17*$^{m-/-,h+}$) mice that we recently produced. First, we generated immunodeficient *Rag-2*$^{-/-}$/COL17–humanized mice by crossing *Rag-2*$^{-/-}$ mice with COL17-humanized mice. Then, splenocytes from wild-type mice that had been immunized by grafting of human COL17-transgenic mouse skin were transferred into *Rag-2*$^{-/-}$/COL17–humanized mice. The recipient mice continuously produced anti-human COL17 IgG Abs in vivo and developed blisters and erosions corresponding to clinical, histological, and immunopathological features of BP, although eosinophil infiltration, one of the characteristic histological findings observed in BP patients, was not detected in the recipients. Although the depletion of CD8$^+$ T cells from the immunized splenocytes was found to produce no effects in the recipients, the depletion of CD4$^+$ T cells as well as CD45R$^+$ B cells was found to inhibit the production of anti-human COL17 IgG Abs in the recipients, resulting in no apparent clinical phenotype. Furthermore, we demonstrated that cyclosporin A significantly suppressed the production of anti-human COL17 IgG Abs and prevented the development of the BP phenotype in the treated recipients. Although this model in an immunodeficient mouse does not exactly reproduce the induction mechanism of BP in human patients, this unique experimental system targeting humanized pathogenic Ag allows us to investigate ongoing autoimmune responses to human molecules in experimental animal models. *The Journal of Immunology*, 2010, 184: 2166–2174.

To investigate the pathogenic mechanisms of autoimmune diseases, the development of animal models is essential (1, 2). However, interspecies molecular differences in autoantigens make it difficult to develop autoimmune animal disease models in some cases. We recently overcame this issue by using the unique technique of humanization of autoantigens to generate an animal model for bullous pemphigoid (BP) (1).

BP is the most common autoimmune blistering disorder that is induced by autoantibodies against type XVII collagen (COL17, also called BP180 or BPAG2), a hemidesmosomal type II transmembrane protein that spans the lamina lucida and projects into the lamina densa of the epidermal basement membrane zone (3–7). The noncollagenous 16A domain located at the membrane-proximal region of COL17 is known as the major pathogenic epitope for BP (8, 9). Our group recently generated COL17-humanized mice (*COL17*$^{m-/-,h+}$) that lack mouse COL17 but express human COL17 (hCOL17) (1). Autoantibodies from BP patients fail to recognize mouse COL17 due to differences in the amino acid sequence between human and mouse. In contrast, BP autoantibodies react to hCOL17 molecules expressed in COL17-humanized mice and induce BP-like skin lesions in the neonates. Thus, this passive-transfer BP mouse model directly demonstrated the pathogenicity of human BP autoantibodies (1). Our system makes it possible to investigate immune reactions mediated by Abs specific to human molecules even in animal models.

However, passive-transfer animal models demonstrate only transient disease activity. In this study, we have developed an active, stable BP model to further advance our knowledge of the BP pathogenic mechanisms for the dynamic process of developing chronic inflammatory skin lesions observed in BP patients. To develop such a model, we adoptively transferred the splenocytes immunized with hCOL17 into immunodeficient COL17-humanized recipients (10). This active, stable autoimmune disease model targeting humanized pathogenic Ag enables us to investigate ongoing autoimmune responses to human molecules in experimental animals.

Materials and Methods

Mice

C57BL/6J mice were purchased from Japan Clea (Hamamatsu, Japan). C57BL/6-background *Rag-2*$^{-/-}$ mice were received as a gift from the Central Institute for Experimental Animals (Kawasaki, Japan). We crossed *COL17*$^{m-/-,h+}$ (COL17-humanized) mice that we had recently generated (1) with *Rag-2*$^{-/-}$ mice. Mice that carried the heterozygous null mutations of both the *Rag-2* and mouse *Col17* genes and the transgene of human *COL17* (*Rag-2*$^{+/-}$/*COL17*$^{m+/-,h+}$) were bred to produce *Rag-2*$^{-/-}$/*COL17*$^{m-/-,h+}$ (*Rag-2*$^{-/-}$/COL17–humanized) mice. All of the animal procedures were conducted according to guidelines provided by the Hokkaido University Institutional Animal Care and Use Committee under an approved protocol.

Department of Dermatology, Hokkaido University Graduate School of Medicine, Sapporo, Japan

Received for publication September 21, 2009. Accepted for publication December 9, 2009.

This work was supported in part by Grants-in-Aid for Scientific Research (A) (No. 21249063 to H.S.) and (C) (No. 20591312 to A.S.) from the Ministry of Education, Culture, Sports, Science and Technology of Japan and by the Program for Promotion of Fundamental Studies in Health Sciences of the National Institute of Biomedical Innovation (No. 06-42 to H.S.).

Address correspondence and reprint requests to Dr. Hiroshi Shimizu and Dr. Akihiko Shibaki, Department of Dermatology, Hokkaido University Graduate School of Medicine, N.15 W.7, Kita-ku, Sapporo 060-8638, Japan. E-mail addresses: shimizu@med.hokudai.ac.jp or ashibaki@med.hokudai.ac.jp

Abbreviations used in this paper: BP, bullous pemphigoid; COL17, type XVII collagen; CsA, cyclosporin A; DEJ, dermal–epidermal junction; hCOL17, human COL17; hNC16A, human COL17 noncollagenous 16A domain; IF, immunofluorescence; LD, lamina densa; Tg, transgenic; Treg, regulatory T cell; WT, wild-type.

www.jimmunol.org/cgi/doi/10.4049/jimmunol.0903101

Immunization of mice by hCOL17*-transgenic skin grafting*

Immunization of the mice by *hCOL17*-transgenic (Tg) skin graft was performed according to the method reported by Olasz et al. (11). Briefly, full-thickness 1-cm^2 pieces of dorsal skin were removed from sacrificed *hCOL17*-Tg mice ($COL17^{m+/+,h+}$) and grafted onto the backs of gender-matched 6-wk-old C57BL/6 wild-type (WT) mice. After topical application of antibiotic ointment, the grafted site was covered with gauze and an elastic bandage for 14 d. In selected experiments, WT mouse skin was grafted onto the backs of WT mice. Ab production was confirmed at 5 wk after skin grafting by indirect immunofluorescence (IF) analysis, as described below.

IF analysis

Indirect IF using mice sera was performed on the skin samples from human, COL17-humanized mice, or WT mice using standard protocols (1). In selected experiments, indirect IF was performed on 1 M NaCl-split normal human skin. We used FITC-conjugated Abs against mouse IgG (Jackson ImmunoResearch Laboratories, West Grove, PA), mouse IgG1, IgG2a, IgG2b, and IgG3 (BD Pharmingen, San Diego, CA), and mouse IgG2c (Bethyl Laboratories, Montgomery, TX) as the secondary Abs.

ELISA

To determine the Ab titer against hCOL17 noncollagenous 16A domain (hNC16A) in the serum samples from the experimental mice, 96-well microtiter plates coated with recombinant hNC16A protein purchased from Medical & Biological Laboratories (Nagoya, Japan) were incubated with diluted mouse sera for 1 h at room temperature. After being washed, bound Abs were developed with a 40,000-fold–diluted, HRP-labeled Ab specific to mouse IgG (Jackson ImmunoResearch Laboratories), and the OD was read at 450 nm using an ELISA plate reader (Mithras; Berthold Technologies, Bad Wildbad, Germany). The ELISA index value was defined by the following formula: index = (OD_{450} of tested serum – OD_{450} of negative control)/(OD_{450} of positive control – OD_{450} of negative control) × 100 (10).

Immunoblotting

Immunoblotting was performed as described previously (1). Recombinant proteins were subjected to SDS-PAGE and electrotransferred onto nitrocellulose membrane (Trans-Blot; Bio-Rad, Hercules, CA). The membranes were blocked and incubated at room temperature for 1 h with diluted sera obtained from experimental mice. After being washed, the membranes were incubated with alkaline phosphatase-conjugated anti-mouse IgG (Zymed Laboratories, South San Francisco, CA). The bound Abs were detected by the Western Blue Stabilized Substrate for Alkaline Phosphatase (Promega, Madison, WI).

Complement fixation study

Complement activation induced by Abs obtained from the immunized WT mice against the COL17 in human skin samples was investigated by IF microscopy as previously described, with minor modifications (12). Cryosections of human skin were incubated with IgG (10 μg/ml) from immunized WT mice for 1 h at 37°C. Freshly prepared mouse serum was then added as a complement source. One hour after incubation, in situ deposition of mouse complement C3 was detected with FITC-conjugated Abs specific to mouse C3 (Cappel; Valeant Pharmaceuticals, Costa Mesa, CA).

Adoptive transfer of splenocytes

Splenocytes were isolated and pooled from several immunized WT mice at 35 d after the skin grafting and administered to *Rag-2*$^{-/-}$/COL17–humanized or *Rag-2*$^{-/-}$ mice by i.v. injection into the tail vein with 2.0 × 10^8 splenocytes in 500 μl PBS per mouse (10).

ELISPOT assay

ELISPOT assay was performed as previously described (10, 13) with some minor modifications. Polyvinylidene difluoride-bottomed 96-well multiscreen plates (Millipore, Bedford, MA) were coated with 30 μg/ml recombinant hNC16A protein. In some experiments, 30 μg/ml recombinant mouse noncollagenous 14A domain protein was coated as negative controls. Mononuclear cells isolated from the spleen, bone marrow, and lymph nodes of the *Rag-2*$^{-/-}$/COL17–humanized recipients were incubated on the plate at 37°C in a 5% CO_2 incubator for 4 h. IgG bound to the membrane was visualized as spots with alkaline phosphatase-conjugated anti-mouse IgG Abs. The number of spots was counted under a dissecting microscope (SMZ1500; Nikon, Tokyo, Japan), and the frequency of anti-hNC16A IgG-producing B cells was defined as the number of spots in 10^5 mononuclear cells.

Evaluation of recipient mice

Weekly, the recipient mice were examined for their general condition and cutaneous lesions (i.e., erythema, hair loss, blisters, erosions, and crusts). Extent of skin disease was scored as follows: 0, no lesions; 1, lesions on <10% of the skin surface; 2, lesions on 10–20% of the skin surface; 3, lesions on 20–40% of the skin surface; 4, lesions on 40–60% of the skin surface; 5, lesions on >60% of the skin surface, as previously described (14) with minor modifications. Serum samples were also obtained from recipient mice weekly and assayed by indirect IF microscopy and hNC16A ELISA. Biopsies of lesional and perilesional skin were obtained between 2 and 5 wk after adoptive transfer for light microscopy (H&E), for toluidine blue staining to evaluate mast cell infiltration and degranulation, and for direct IF using FITC-conjugated Abs against mouse IgG, IgG1, IgG2a, IgG2b, IgG2c, IgG3, and C3.

Immunoelectron microscopy

Postembedding immunoelectron microscopy of cryofixed and cryosubstituted skin samples taken from the *Rag-2*$^{-/-}$/COL17–humanized mice at 5 wk after the adoptive transfer of immunized splenocytes was performed as previously described (15, 16) with minor modifications. Small pieces of fresh skin were cryofixed by plunging them into liquid propane at −190°C using a freeze–plunge apparatus (Leica Microsystems, Cambridge, U.K.). Skin samples were then cryosubstituted with methanol at −80°C using an automated freeze substitution system (Leica Microsystems) and embedded in Lowicryl K11M (Ladd Research Industries, Williston, VT) at −60°C. Ultrathin sections were incubated with 5-nm gold-labeled goat anti-mouse IgG (Biocell Laboratories, Rancho Dominguez, CA) and observed with a transmission electron microscope (H-7100; Hitachi High-Technologies, Tokyo, Japan).

Preparation of IgG fractions from mice and passive-transfer studies

Sera were obtained from *Rag-2*$^{-/-}$/COL17–humanized mice at 8 d after the adoptive transfer of immunized splenocytes. Total IgG was prepared from the sera by affinity chromatography using a HiTrap Protein G HP (GE Healthcare Biosciences, Uppsala, Sweden). We performed passive transfer of IgG into mice as previously described (1). A 60-μl dose of sterile IgG in PBS was administered to neonatal COL17-humanized mice by i.p. injection (0.1, 0.5, or 1.0 mg/g body weight). As a control, we prepared the total IgG fractions from WT mice and i.p. injected them into neonatal COL17-humanized mice (1.0 mg/g body weight). We judged skin phenotype at 48 h after the injection. The animals were then sacrificed, and skin sections were taken for histological examination.

Depletion of $CD4^+$ or $CD8^+$ T cells or $CD45R^+$ B cells from immunized splenocytes

For adoptive transfer of immunized splenocytes without $CD4^+$ or $CD8^+$ T cells or $CD45R^+$ B cells, we depleted each fraction from splenocytes of the immunized WT mice by using microbeads conjugated to monoclonal anti-mouse CD4 (L3T4), anti-mouse CD8a (Ly-2), or anti-mouse CD45R (B220) Abs (Miltenyi Biotec, Auburn, CA). The depletions of $CD4^+$ or $CD8^+$ T cells or $CD45R^+$ B cells were confirmed by flow cytometric analysis on a FACSAria (BD Pharmingen) as described below. Approximately 1.0 to 2.0 × 10^8 splenocytes depleted with $CD4^+$ or $CD8^+$ T cells or $CD45R^+$ B cells were adoptively transferred to *Rag-2*$^{-/-}$/COL17–humanized mice.

Administration of cyclosporin A to the BP model mice

Cyclosporin A (CsA) (Novartis Pharma, Basel, Switzerland) dissolved in olive oil was given i.p. at the dose of 35 mg/kg (100 μl) from 2 d after the adoptive transfer and continued daily for 14 d. The dose was chosen based on a previous study (17) and our preliminary data. As a control, the same volume of olive oil was injected into the BP model mice. The treated BP model mice were observed for 5 wk to evaluate the efficacy of the treatments.

Flow cytometry

The following mAbs were purchased from BD Pharmingen: 145-2C11-FITC (anti-CD3ε), H129.19-FITC (anti-CD4), 53-6.7-PE (anti-CD8), and RA3-6B2-PE (anti-CD45R/B220). One million cells were stained and subjected to analysis using a FACSAria.

Statistical analysis

To compare ELISA index values of Abs, the weights of mice, and the numbers of splenocytes, Student *t* tests were applied. We determined the statistical differences between groups of indirect IF titer and disease severity using the

Mann-Whitney U test or ANOVA with the Scheffe F test. Data were expressed as mean ± SE. We considered p values of <0.05 as significant.

Results

High titer of anti-hCOL17 IgG is induced in WT mice by hCOL17-Tg skin graft immunization

To induce anti-hCOL17 IgG Abs, WT mice were immunized by skin grafting from *hCOL17*-Tg mice, which express hCOL17 in the epidermis under the control of the human keratin 14 promoter (1, 11, 18). As reported by Olasz et al. (11), a high titer of IgG Abs specific to hNC16A was produced within 5 wk after the skin grafting. Levels of IgG Abs specific to hNC16A were measured by ELISA. The ELISA index values of sera from WT mice immunized by *hCOL17*-Tg skin grafting showed significantly higher reactivity than those values of sera from control WT skin-grafted WT mice (74.9 ± 13.5 versus 1.5 ± 1.0, $p < 0.01$) (Fig. 1*A*). Immune serum was analyzed by indirect IF, which revealed the deposition of IgG Abs at the dermal–epidermal junction (DEJ) of COL17-humanized mouse skin (Fig. 1*B*). There was no reactivity against WT mouse skin (Fig. 1*C*). We prepared the IgG fractions of sera from WT mice immunized by COL17-Tg skin grafting by affinity chromatography and determined the complement-fixing activity of purified IgG by indirect IF analysis. We found that 10 μg purified IgG could fix mouse C3 contained in freshly prepared mouse serum to the DEJ of normal human skin, whereas mouse C3 without purified IgG could not bind to the DEJ (Fig. 1*D*, 1*E*). The IgG subclass of anti-hCOL17 Abs present in the serum of each WT mouse immunized by *hCOL17*-Tg skin grafting was assessed by indirect IF analysis ($n = 10$). The deposition of IgG1, IgG2a, IgG2b, IgG2c, or IgG3 at the DEJ of normal human skin was observed in 100, 20, 10, 70, or 0% of the analyzed sera, respectively. Thus, immunized WT mice produce high titers of IgG1 and IgG2c anti-hCOL17 Abs that have complement-fixing activity.

Splenocytes transferred from the immunized mice produce a high titer of pathogenic anti-hCOL17 IgG Abs in the Rag-$2^{-/-}$/*COL17–humanized recipients*

To develop an active disease model for BP targeting humanized pathogenic Ag, we generated immunodeficient *Rag-*$2^{-/-}$/COL17–humanized (*Rag-*$2^{-/-}$/*COL17*$^{m-/-,h+}$) mice. First, we crossed COL17-humanized (*COL17*$^{m-/-,h+}$) mice with immunodeficient *Rag-*$2^{-/-}$ mice to generate *Rag-*$2^{+/-}$/*COL17*$^{m+/-,h+}$ mice. Next, those *Rag-*$2^{+/-}$/*COL17*$^{m+/-,h+}$ mice were crossed with each other, and the genotypes of the offspring were carefully screened. After four to five repeated crossings, we finally obtained the *Rag-*$2^{-/-}$/COL17–humanized mice. As a next step, splenocytes from some of the immunized WT mice were pooled after isolation and then adoptively transferred into the *Rag-*$2^{-/-}$/COL17–humanized mice that expressed hCOL17 protein in vivo ($n = 10$). Because these *Rag-*$2^{-/-}$/COL17–humanized mice had no mature T or B cells, they were able to accept the transferred splenocytes. All of the *Rag-*$2^{-/-}$/COL17–humanized recipients that were given immunized splenocytes produced IgG Abs against hCOL17 (Fig. 2*C*, 2*D*, Table I). Indirect IF examination revealed that IgG Abs produced in the recipients bound to the DEJ of normal human skin and COL17-humanized mouse skin but not to WT mouse skin. IF analysis using 1 M NaCl-split normal human skin as a substrate showed linear deposition of IgG on the epidermal side (Fig. 2*A*). Immunoblot analysis revealed that the recipients' sera reacted with both recombinant hCOL17 and hNC16A (Fig. 2*B*). Time-course analysis revealed that anti-DEJ IgG, which reflects the presence of anti-hCOL17 IgG, became detectable in recipients' sera within 1 wk after the transfer and that the titer peaked around

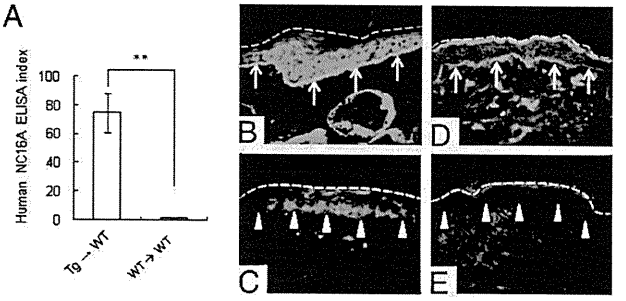

FIGURE 1. Circulating IgG Abs in the WT mice immunized by *hCOL17*-Tg skin grafting (immunized WT mice) recognize recombinant hNC16A and the DEJ of COL17-humanized mouse skin and activate mouse complement C3 in vitro. *A*, Anti-hNC16A IgG Abs are measured by ELISA. The index values of sera from immunized WT mice (Tg → WT) demonstrate significantly higher reactivities than those of sera from WT mice grafted with WT skin (WT → WT). *B* and *C*, The sera from immunized WT mice show positive reaction at the DEJ of COL17-humanized mouse skin (arrows) (*B*) but no specific reaction in WT mouse skin (arrow heads) (*C*) by indirect IF microscopy (original magnification ×200). *D* and *E*, Purified IgG from the immunized WT mice is able to fix mouse C3 to the DEJ (arrows) (*D*); no significant complement fixation is observed without the purified IgG from the immunized WT mice (arrow heads) (*E*). FITC-conjugated anti-mouse C3 Ab is used for the analysis (original magnification ×200). $^{**}p < 0.01$

day 9 after the transfer. Although the titer gradually decreased after the peak, it remained high (>5120×) for >10 wk without boosting (Fig. 2*C*). ELISA analysis revealed that anti-hNC16A IgG Abs appeared in the recipients' sera as early as 1 wk after the transfer. The Ab level rapidly increased, peaking around day 9 after the transfer. Although the titer gradually decreased, falling to a stable level at 6 wk after the transfer, anti-hNC16A IgG Abs were detectable for >10 wk without boosting (Fig. 2*D*). These results demonstrate that splenocytes from immunized WT mice can survive in the *Rag-*$2^{-/-}$/COL17–humanized recipients and produce a high titer of anti-hCOL17 Abs containing IgG against hNC16A. ELISPOT assay revealed that anti-hNC16A IgG-producing B cells in the *Rag-*$2^{-/-}$/COL17–humanized recipients existed mainly in the spleen and lymph nodes but not in bone marrow at days 9 and 10. Although the number of anti-hNC16A IgG-producing B cells decreased at day 52, it still remained detectable (Table II).

As a control, immunized splenocytes were also transferred into *Rag-*$2^{-/-}$ mice ($n = 6$). Interestingly, neither anti-DEJ nor anti-hNC16A IgG Abs were detected in control *Rag-*$2^{-/-}$ recipients (Fig. 2*C*, 2*D*, Table I). To exclude the possibility that transferred splenocytes cannot survive in the *Rag-*$2^{-/-}$ recipients, we grafted *hCOL17*-Tg skin onto the *Rag-*$2^{-/-}$ recipients 5 wk after the adoptive transfer of immunized splenocytes ($n = 3$). A high titer of anti-hCOL17 IgG Abs was detected within 14 d after the skin grafting in the *Rag-*$2^{-/-}$ recipients (data not shown). These results demonstrate that splenocytes transferred from the immunized WT mice can produce a high titer of anti-hCOL17 IgG Abs in the *Rag-*$2^{-/-}$/COL17–humanized recipients but not in the *Rag-*$2^{-/-}$ recipients.

Rag-$2^{-/-}$/*COL17–humanized mice given immunized splenocytes develop the BP phenotype*

The phenotypes observed in the recipient mice are summarized in Table I. Around day 7 after the adoptive transfer, the *Rag-*$2^{-/-}$/5COL17–humanized recipients began to scratch their snouts, muzzles, ears, and chests. Patchy hair loss associated with erythema began to develop on the chest between 9 and 14 d after the

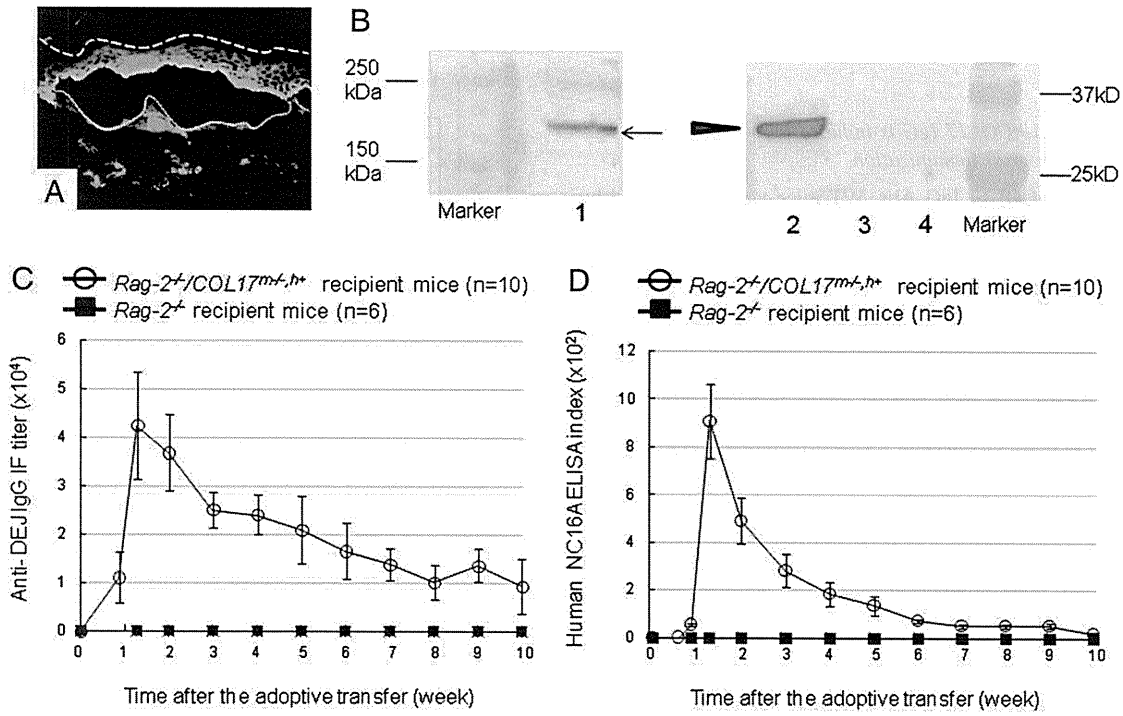

FIGURE 2. *Rag-2*$^{-/-}$/COL17–humanized mice given immunized splenocytes produce anti-hCOL17 Abs in vivo. *A*, Sera from the *Rag-2*$^{-/-}$/COL17–humanized recipients react to the epidermal side of 1 M NaCl-split normal human skin in indirect IF microscopy (original magnification ×200). *B*, IgG purified from a *Rag-2*$^{-/-}$/COL17–humanized recipient serum binds to 180-kDa recombinant hCOL17 (*lane* 1) and 35-kDa recombinant hNC16A proteins (*lane* 2) but fails to bind to recombinant mouse noncollagenous 14A domain, corresponding to hNC16A (*lane* 3) or GST proteins (*lane* 4). *C*, Persistent production of anti-DEJ IgG Abs in the *Rag-2*$^{-/-}$/COL17–humanized recipients is detected by indirect IF analysis. The titers rapidly increase and peak around day 9 after the transfer, and then they gradually decrease. In contrast, no anti-DEJ IgG Abs are detected in control *Rag-2*$^{-/-}$ recipients (n = 10; controls, n = 6). *D*, The IgG titers of sera from the *Rag-2*$^{-/-}$/COL17–humanized recipients and control *Rag-2*$^{-/-}$ recipients were measured by recombinant hNC16A ELISA. The titers rapidly increased after the transfer, peak around 1 wk, and then gradually decrease, stabilizing at a low level 6 wk after the transfer. No anti-hNC16A IgG Abs are observed in control *Rag-2*$^{-/-}$ recipients (n = 10; controls, n = 6).

adoptive transfer in most of the recipients. Then, blisters and erosions spontaneously developed in the dehaired areas on the trunk (Fig. 3*A*). Genital erosions and ears swelling with crusts were also observed (Fig. 3*B*, 3*C*). The dehaired patches gradually enlarged and spread to other regions on the trunk over the next 2–4 wk, resulting in large areas of alopecia (Fig. 3*D*, 3*E*). The epidermis on the trunk and tail easily detached from the dermis by gentle friction (Fig. 3*F*, 3*G*). Disease severity, scored by the percentage of skin surface with the BP phenotype (14), plateaued 5 wk after the transfer (Fig. 4). Conversely, none of the control *Rag-2*$^{-/-}$ recipients developed any skin lesions (Fig. 4). Also, splenocytes from untreated WT mice produced very low levels of anti-hCOL17 and anti-hNC16A IgG Abs and failed to induce any phenotypic changes in the *Rag-2*$^{-/-}$/COL17–humanized recipients (data not shown). In addition, 3 out of 10 *Rag-2*$^{-/-}$/COL17–humanized recipients showed changes on <20% of the skin surface (Table I). In one of those three recipients, the index value of the hNC16A ELISA at day 9 was far lower than the average (85.3 versus 907.8), whereas the anti-hCOL17 IgG titer at day 9 checked by indirect IF analysis was similar to the average. The other two recipients with changes of <20% of the surface showed no obvious difference in the IgG titers compared with the average. Long-term follow-up of

Table I. *Summary of phenotypes observed in recipient mice*

Donor	Recipient	n	Serum Abs		Subepidermal Separation in H&E Staining	Mast Cell Degranulation in Toluidine Blue Staining	Skin Immunopathology[c]		Skin Changes[d]
			IF[a]	ELISA[b]			IgG	C3	
C57BL/6 immunized by Tg[e] skin grafting	*Rag-2*$^{-/-}$/*COL17*$^{m-/-,h+}$	10	10/10	10/10	8/10	10/10	10/10	10/10	7/10
C57BL/6 immunized by Tg[e] skin grafting	*Rag-2*$^{-/-}$	6	0/6	0/6	0/6	0/6	0/6	0/6	0/6

[a]Linear deposition of IgG at the DEJ of the skin was detected by indirect IF microscopy on normal human skin cryosections using 40-fold–diluted recipient mouse serum obtained 2 wk after the adoptive transfer of splenocytes.
[b]Circulating IgG was tested with ELISA against recombinant hNC16A protein using 300-fold–diluted mouse serum obtained 2 wk after the adoptive transfer. The cutoff index value was set at 20.
[c]In vivo IgG and complement C3 deposition at the DEJ of the skin was determined by direct IF of perilesional skin biopsies. Medium or intense staining was regarded as positive.
[d]Skin changes including erythema, hair loss, bullae, and erosions exceeding 20% of the skin surface were considered significant.
[e]Tg: *hCOL17*-transgenic. The recipients in this table are those shown in Figs. 2*C*, 2*D*, and 4.

Table II. *ELISPOT assay of the anti-hNC16A IgG-producing B cells*

Mouse	Day[a]	Spleen	Lymph Node	Bone Marrow
#488	9	135 ± 16.2	43.5 ± 4.0	2 ± 0.8
#109	10	70.5 ± 5.4	84.0 ± 10.5	3.8 ± 0.6
#805	52	17.0 ± 2.7	10.5 ± 2.3	1.7 ± 0.2

Rag-2$^{-/-}$*/COL17*$^{m-/-,h+}$ mice were transferred with splenocytes of the immunized WT mice. The number of the anti-hNC16A IgG-producing B cells is displayed per 10^5 cells in spleen, lymph nodes, and bone marrow.

[a]Number of days after the transfer of immunized splenocytes.

BP model mice demonstrated a trend in which the disease severity started to decrease around 12 wk after the transfer; however, there was variation among the individual mice.

Histopathologic analysis of the lesional skin demonstrated the dermal–epidermal separation associated with mild inflammatory cell infiltration (Fig. 3*H*). Mast cell degranulation was observed in the dermis in toluidine blue staining (Fig. 3*I*). In the control *Rag-2*$^{-/-}$ recipients, no significant histopathologic changes were detected (Table I). Direct IF analysis of perilesional skin biopsies revealed linear deposition of IgG (Fig. 3*J*) and C3 (Fig. 3*K*) at the DEJ in all of the *Rag-2*$^{-/-}$/COL17–humanized recipients, whereas no IgG deposition was detected in the control *Rag-2*$^{-/-}$ recipients (Table I). Time-course analysis of the in situ deposition of IgG Abs in the *Rag-2*$^{-/-}$/COL17–humanized recipients ($n = 3$) by direct IF at days 4, 9, 14, and 21 demonstrated intense deposition of anti-hCOL17 IgG Abs at the DEJ as early as day 9 after the adoptive transfer, and the same levels of deposition were observed at days 14 and 21.

The subclasses of IgG produced in the *Rag-2*$^{-/-}$/COL17–humanized recipients were also analyzed by direct IF ($n = 10$). All of the *Rag-2*$^{-/-}$/COL17–humanized recipients showed a positive reaction with IgG1, IgG2a, IgG2b, and IgG2c Abs at the DEJ. Immunogold electron microscopy of the perilesional skin in the *Rag-2*$^{-/-}$/COL17–humanized recipients showed that anti-mouse IgG Abs were located on and around the plasma membrane of the basal cells (Fig. 3*L*), suggesting that Abs produced in the recipients bind to hCOL17.

To further confirm the pathogenicity of IgG Abs produced in the *Rag-2*$^{-/-}$/COL17–humanized recipients, we purified IgG from the sera obtained from the *Rag-2*$^{-/-}$/COL17–humanized recipients at 8 d after the adoptive transfer and passively transferred them into COL17-humanized neonatal mice by i.p. injection. Transferred neonatal mice developed erythema around the injection site and epidermal detachment by gentle friction at 48 h after the injection (0.1, 0.5, or 1.0 mg/g body weight, $n = 5$, respectively) (Fig. 5*A*). Histopathologic examination of the lesional skin revealed separation between the epidermis and the dermis, with infiltration of inflammatory cells (Fig. 5*B*). Mast cell degranulation in the dermis was also observed in toluidine blue staining (Fig. 5*C*). Direct IF examinations revealed linear deposition of mouse IgG and C3 at the DEJ (Fig. 5*D*, 5*E*). In contrast, the recipient mice that received 1.0 mg/g body weight of IgG purified from WT mice showed no skin detachment, nor any histologic or immunopathologic changes ($n = 5$) (Fig. 5*F–J*). These findings show that IgG Abs purified from the *Rag-2*$^{-/-}$/COL17–humanized recipients are capable of inducing subepidermal blistering in COL17–humanized neonatal mice, which is associated with the binding of IgG Abs to the DEJ, followed by in situ activation of mouse complement and mast cell degranulation.

CD4$^+$ *T cells as well as CD45R*$^+$ *B cells are essential for the stable production of anti-hCOL17 IgG Abs in the* Rag-2$^{-/-}$/*COL17–humanized recipients*

To determine the pathogenic roles of T cells and B cells in the *Rag-2*$^{-/-}$/COL17–humanized recipients, we depleted CD4$^+$ or CD8$^+$ T cells or CD45R$^+$ B cells from splenocytes of the immunized WT

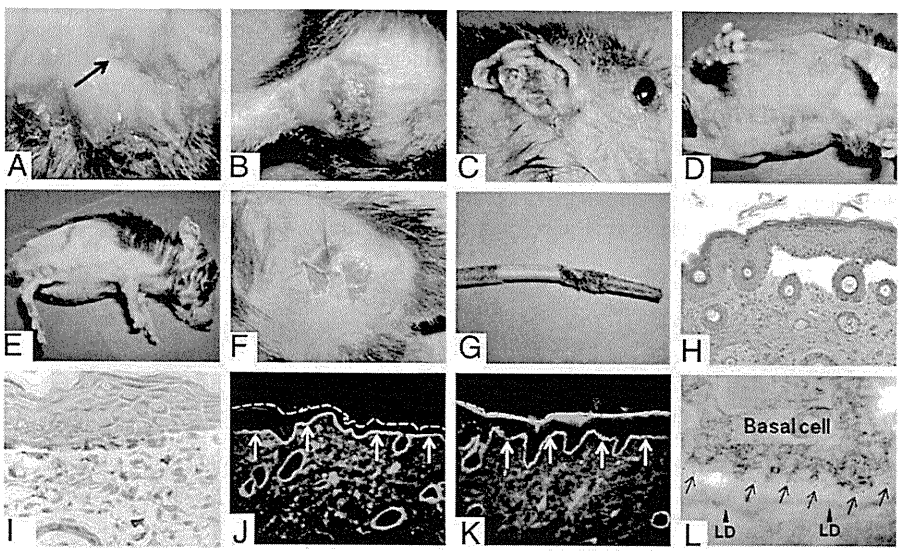

FIGURE 3. *Rag-2*$^{-/-}$/COL17–humanized mice given immunized splenocytes demonstrate the BP phenotype associated with histologic and immunopathologic changes similar to BP. *A*, Spontaneously developing blisters are observed in the *Rag-2*$^{-/-}$/COL17–humanized recipients 3 wk after the transfer (arrow). *B* and *C*, Genital erosions and ear swelling with crusts are seen in the recipients. *D* and *E*, Large, diffuse patches of hair loss associated with erythema, erosions, and crusts on the trunk and the paws. *F* and *G*, Epidermal detachment by gentle friction on the trunk and tail is characteristically observed. *H*, Histologic examination of diseased mice reveals separation between dermis and epidermis with mild inflammatory cell infiltration in H&E staining (original magnification ×200). *I*, Mast cell degranulation in the dermis is observed in toluidine blue staining (original magnification×400). *J* and *K*, Direct IF analysis of lesional skin biopsy reveals linear deposition of mouse IgG (arrows) (*J*) and mouse C3 (arrows) (*K*) along the DEJ (original magnification ×200). *L*, Immunoelectron microscopy demonstrates that mouse IgG Abs deposit at the DEJ close to the plasma membranes of basal cells in the skin of the *Rag-2*$^{-/-}$/COL17–humanized recipient (arrows). LD, lamina densa.

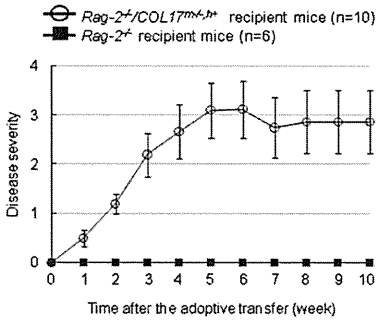

FIGURE 4. *Rag-2$^{-/-}$*/COL17–humanized mice given immunized splenocytes develop the BP disease phenotype. Disease severities of the *Rag-2$^{-/-}$*/COL17–humanized recipients gradually increase, plateauing 5 wk after the transfer. None of the control *Rag-2$^{-/-}$* recipients develop any skin lesions (n = 10; controls, n = 6). Disease severity is scored as described in *Materials and Methods*.

mice and adoptively transferred them into the *Rag-2$^{-/-}$*/COL17–humanized mice. All of the recipient mice given immunized splenocytes after the depletion of CD8$^+$ T cells produced a high titer of anti-hCOL17 IgG Abs and developed severe BP lesions associated with histopathologic and immunopathologic changes indistinguishable from those of the *Rag-2$^{-/-}$*/COL17–humanized mice given whole immunized splenocytes (n = 4) (Fig. 6). In contrast, the depletion of CD4$^+$ T cells or CD45R$^+$ B cells inhibited the production of anti-hCOL17 IgG Abs and the development of the BP phenotype (n = 4, respectively) (Fig. 6). These findings indicate that CD4$^+$, but not CD8$^+$, T cells and CD45R$^+$ B cells are crucial for the production of anti-hCOL17 IgG Abs and for the development of the BP phenotype.

To further investigate the pathogenic role of CD4$^+$ T cells in the *Rag-2$^{-/-}$*/COL17–humanized recipients, we examined the efficacy of CsA (19–22). Approximately 35 mg/kg of CsA dissolved in olive oil (n = 5) or a control vehicle (n = 5) was i.p. injected into the *Rag-2$^{-/-}$*/COL17–humanized recipients from 2 d after the adoptive transfer of whole immunized splenocytes, once daily for 14 d. When the numbers of splenocytes at day 9 after the transfer were compared, the mean number of splenocytes in both groups was not significantly different (8.3×10^7 cells in the CsA-treated mice versus 11.0×10^7 cells in the control mice, $p > 0.05$). Although the mean percentage of CD3$^+$ T cells was significantly lower in the CsA-treated mice than that in the control mice (14.1% in the CsA-treated mice versus 24.5% in the control mice, $p < 0.05$), the mean percentages of CD45R$^+$ B cells were similar in both groups (28.8% in the CsA-treated mice versus 26.5% in the control mice, $p > 0.05$). Disease severity and the titers of circulating anti-hNC16A IgG Abs were significantly lower in the treated mice than those in the controls (Fig. 7). This result further suggests that CD4$^+$ T cells play a pivotal role in the pathogenesis of this BP model.

Discussion

This is the first active BP model that stably produces pathogenic anti-hCOL17 Abs and spontaneously develops blisters and erosions on the skin. Because amino acid sequences of COL17, especially those of the noncollagenous 16A domain region, are different between human and mouse, an animal model using COL17-humanized mice that express hCOL17 is suitable for analyzing pathogenic mechanisms of human BP. Therefore, we developed an active BP model in which the targeted pathogenic Ag is hCOL17 but not mouse COL17. Immunized splenocytes transferred into immunodeficient *Rag-2$^{-/-}$*/COL17–humanized recipients survived and continuously produced a high titer of anti-hCOL17 Abs in vivo for >10 wk after the adoptive transfer. Those Abs bound to the hCOL17 molecules that were expressed in the recipients' skin, which initiated subsequent immune reactions including complement activation and mast cell degranulation, resulting in dermal–epidermal separation. This array of immune responses was consistent with the pathogenic mechanisms of BP previously demonstrated in passive-transfer neonatal mouse models (1, 12, 23–25). Furthermore, the *Rag-2$^{-/-}$*/COL17–humanized recipients developed blisters and erosions on erythematous skin areas that lasted >10 wk. The pathogenicity of anti-hCOL17 IgG Abs was confirmed by passive-transfer experiments that revealed that IgG Abs obtained from the *Rag-2$^{-/-}$*/COL17–humanized recipients could induce the BP phenotype in COL17-humanized neonatal mice. Thus, pathogenic anti-hCOL17 IgG Abs produced in the *Rag-2$^{-/-}$*/COL17–humanized recipient binds to the target Ag in vivo and induces the BP phenotype. By using COL17-humanized mice, we can observe the dynamic immune reactions induced by pathogenic Abs against hCOL17 molecules. These strategies for the production of active autoimmune disease models targeting humanized pathogenic Ag can also be applied to other autoimmune diseases.

In BP, complement activation is considered to be critical for blister formation (26). The first evidence suggesting the pathogenic role of complements in BP is the demonstration of C3

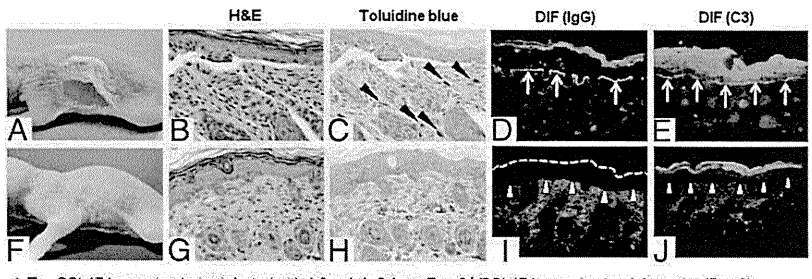

FIGURE 5. COL17-humanized neonatal mice injected with IgG purified from the *Rag-2$^{-/-}$*/COL17–humanized recipients at 8 d after the adoptive transfer show skin fragility and histologic and immunopathologic changes similar to BP. *A*, The recipient mice develop epidermal detachment by gentle friction at 48 h after injection of the 1.0 mg/g IgG purified from the *Rag-2$^{-/-}$*/COL17–humanized recipients (n = 5). *B*, Histologic examination reveals subepidermal separation associated with mild inflammatory cell infiltrates in H&E staining (original magnification ×200). *C*, Mast cell degranulation in the dermis (arrow heads) is observed in toluidine blue staining (original magnification ×400). *D* and *E*, Direct IF studies show linear deposition of mouse IgG (arrows) (*D*) and C3 (arrows) (*E*) at the DEJ (original magnification ×200). *F–J*, No phenotypic or histological findings are observed in the mice injected with 1.0 mg/g IgG purified from sera of WT mice grafted with WT skin (n = 5).

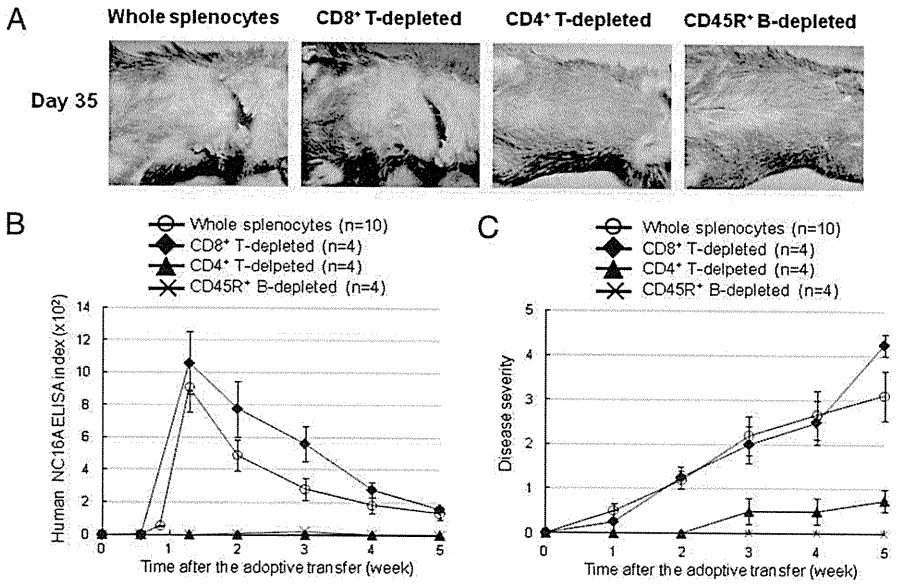

FIGURE 6. The production of anti-hCOL17 IgG Abs requires $CD4^+$ T cells and $CD45R^+$ B cells but not $CD8^+$ T cells. *A*, All of the recipients given $CD8^+$ T cell-depleted splenocytes (n = 4) develop severe BP lesions similar to those of the recipients given whole splenocytes, whereas the recipients given $CD4^+$ T cell-depleted splenocytes (n = 4) or $CD45R^+$ B cell-depleted splenocytes (n = 4) demonstrate no erosive lesions. *B*, The depletions of $CD4^+$ T cells or $CD45R^+$ B cells significantly inhibit the production of anti-hNC16A IgG Abs ($p < 0.01$ at day 9). *C*, The recipients given $CD4^+$ T cell-depleted or $CD45R^+$ B cell-depleted splenocytes show significantly lower disease severities than those in other groups ($p < 0.05$ at days 14 and 35).

deposition at the basement membrane zone of the lesional and perilesional skin by direct IF (27). By means of the passive-transfer experiments using C5-deficient mice, Liu et al. (25) further showed that complement activation is a pivotal step in subepidermal blister formation triggered by rabbit anti-mouse COL17 IgG Abs in their BP animal model. Consistent with these previous studies, linear deposition of complement C3 was observed at the DEJ in all of the diseased *Rag*-$2^{-/-}$/COL17–humanized recipients. We also demonstrated that sera from both the immunized WT mice and the *Rag*-$2^{-/-}$/COL17–humanized recipients contained complement-fixing Abs of the IgG2 subclass and could fix compliments at the DEJ of the normal human skin and the COL17-humanized skin. Analysis of the subclass distribution of IgG autoantibodies in human BP revealed that complement-fixing IgG1 was present as the predominant subclass of autoantibodies (28). These findings suggest that complement activation mediated by Abs of the IgG2 subclass against hCOL17 may induce blister formation in the present BP model.

It is unclear why the anti-hCOL17 IgG titer decreases in a short period. To examine the possible compartmentalization of anti-hCOL17 IgG response to the skin, we checked in situ deposition of anti-hCOL17 IgG in the skin of BP model mice by direct IF analysis sequentially at days 4, 9, 14, and 21. Intense deposition of anti-hCOL17 IgG Abs was detected at the DEJ as early as day 9 of the adoptive transfer, and the same levels of deposition were observed at days 14 and 21 (n = 3). This indicates that the compartmentalization of the anti-hCOL17 IgG response to the skin is not the main reason for the spontaneous reduction of the anti-hCOL17 IgG titer in this BP model. Alternatively, some regulatory mechanism against hCOL17-specific T cells, B cells, or both may be induced in this BP model. In experimental autoimmune myasthenia gravis, an autoimmune neuromuscular disease model induced by anti-acetylcholine receptor Abs, regulatory T cells (Tregs) generated ex vivo or expanded in vivo suppress pathogenic T cell and Ab responses (29, 30). In experimental autoimmune encephalomyelitis, a myelin-reactive T cell-dependent multiple

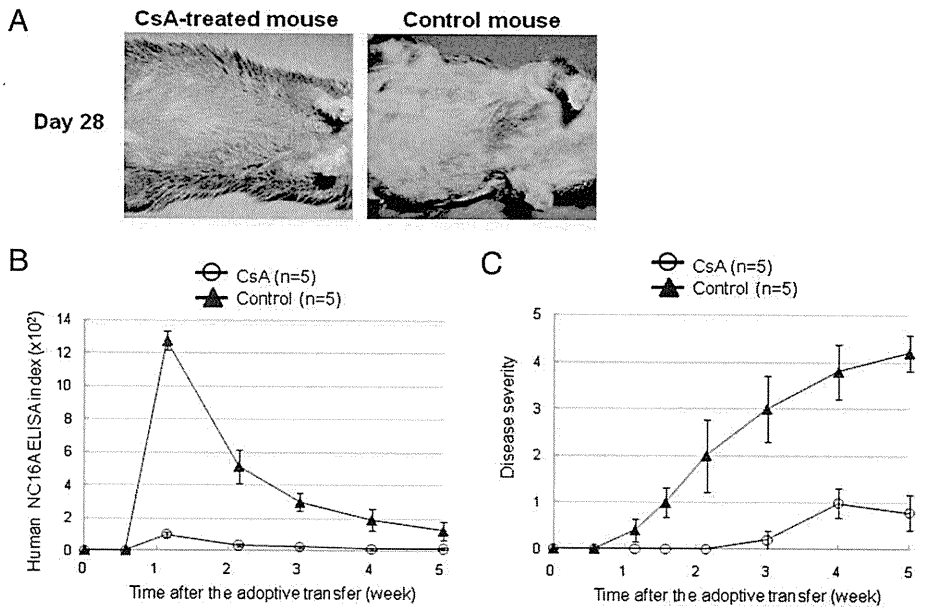

FIGURE 7. Results of CsA treatment in the *Rag*-$2^{-/-}$/COL17–humanized recipients. Approximately 35 mg/kg CsA was administered daily from 2 d after the adoptive transfer for 14 d (CsA, n = 5; control vehicle, n = 5). *A*, Skin lesions of the *Rag*-$2^{-/-}$/COL17–humanized recipients treated with CsA are markedly diminished with CsA treatment (day 28). *B*, CsA significantly suppresses the production of anti-hNC16A IgG ($p <$ 0.01 at days 8, 15, and 21). *C*, The treated mice show significantly lower disease severity than that of the controls ($p < 0.01$ at days 8, 15, 21, 28, and 35).

sclerosis model, natural resolution correlates with the accumulation of myelin-reactive Tregs expanded during the course of experimental autoimmune encephalomyelitis in the inflamed CNS (31, 32). Similar to these autoimmune disease models, Tregs may contribute to the spontaneous decline of the anti-hCOL17 IgG titer in this BP model. Further studies examining Treg function in this BP model may provide clues for controlling the autoimmune reaction in BP patients.

Interestingly, none of the control *Rag-2*$^{-/-}$ recipients given immunized splenocytes produced anti-hCOL17 IgG Abs or developed the BP phenotype despite the presence of living splenocytes in vivo. We further demonstrated that the grafting of *hCOL17*-Tg skin onto *Rag-2*$^{-/-}$ mice 5 wk after the adoptive transfer of immunized splenocytes could induce a high titer of anti-hCOL17 IgG Abs. These results indicate that transferred splenocytes need endogenous hCOL17 molecules to produce anti-hCOL17 IgG Abs. In addition, the depletion of CD4$^+$ T cells from the immunized WT splenocytes suppressed the production of anti-hCOL17 IgG Abs, whereas the depletion of CD8$^+$ T cells showed no effects. This clearly suggests that CD4$^+$ T cells, and not CD8$^+$ T cells, are essential for the production of Abs against hCOL17 in this BP model.

Generally, the production of Abs by B cells requires the help of CD4$^+$ T cells. In experimental autoimmune myasthenia gravis, both MHC class II gene-disrupted mice and CD4 gene knockout mice have been proven to be resistant to induction of clinical experimental autoimmune myasthenia gravis (33, 34). In experimental pemphigus vulgaris, an autoimmune blistering disease caused by anti-desmoglein 3 Abs, the production of autoantibodies required both CD4$^+$ T cells and B cells from naive desmoglein 3 knockout mice (35). To further investigate the pathogenic role of CD4$^+$ T cells, we administered CsA, an immunosuppressant that inhibits T cell function, to the *Rag-2*$^{-/-}$/COL17–humanized recipients after the adoptive transfer of immunized splenocytes. Because active disease models possess more persistent disease activity than passive-transfer neonatal disease models (10, 36, 37), we can easily analyze the time-course changes of disease activity altered by such an intervention. CsA significantly suppressed the production of anti-hNC16A IgG Abs and diminished the disease severity. These results strongly suggest that CD4$^+$ T cells play a pivotal role in the production of the autoantibodies through the presentation of the endogenous autoantigen. In human BP, the presence of autoreactive CD4$^+$ T cells has been reported, indicating the contribution of CD4$^+$ T cells to the pathogenesis of human BP (38–40). In addition, particular MHC class II alleles are more frequent in BP patients (41). These results further indicate that the autoreactive CD4$^+$ T cells may be activated through an interaction with the specific MHC class II molecule in BP. The pathogenic function of CD4$^+$ T cells shown in this BP model may provide a new insight into the pathogenic mechanism of BP and the development of a novel therapeutic strategy that targets T cell-mediated immune reactions.

Although this BP model is a useful tool for investigating the pathophysiology of BP, limitations are still present in our experimental system. First, the induction phase of the autoimmune response, such as the breakdown of self-tolerance, cannot be investigated in this BP model because the immune response to hCOL17 is induced by adoptive transfer of immunized WT splenocytes. To investigate the induction of autoimmunity in BP, Xu et al. (42) have aimed to induce autoimmune responses to mouse COL17 by using the immunocompetent BALB/c mice. Multiple immunizations of BALB/c mice with peptides of the hNC16A domain, its mouse equivalent, or both successfully induced anti-mouse COL17 IgG Abs, although no overt skin changes were observed. Similar experiments have been performed to establish an animal model for epidermolysis bullosa acquisita, a subepidermal blistering disorder induced by Abs against type VII collagen, another hemidesmosomal protein present at the basement membrane zone (43). Anti-type VII collagen Abs and subepidermal blisters were successfully induced in the mice by repeated immunizations with recombinant mouse type VII collagen protein mixed with adjuvant, although the development of the disease phenotype depended on the strain of mice. These results indicate that repeated exposure of the self Ag in conjunction with inflammatory stimulation, such as by bacterial components, may break down peripheral tolerance and induce autoantibody production in patients with a specific genetic background. This concept is further supported by the clinical findings that BP develops preferentially in elderly people and that particular HLA class II alleles correlate with BP patients (41). Second, this BP model demonstrates immune responses against a humanized Ag of the skin; however, the response still occurs in a murine milieu. The lack of eosinophilic infiltration, a characteristic trait of human BP, in this model could be related to the difference of the effector cell function between human and mouse immune systems. Furthermore, because the MHCs in mice are different from those in humans, MHC-dependent presentation of the pathogenic Ag to the T and B cells cannot be simulated in this current BP mouse model. To overcome these issues, not only the pathogenic Ag but also the immune system should be humanized in experimental animals. Recently, quasi-human immune systems have been stably reconstituted in supra-immunodeficient NOG mice using human CD34$^+$ stem cells from various sources including bone marrow, umbilical cord blood, and peripheral blood (44, 45). This system has become a common tool for studying human immunity and diseases relating to it (46, 47). However, even in that system the development of human B cells was partially blocked, and the human T cells lost their function in the periphery (48). Further technical advances would be required to establish more accurate and reliable humanized animal models that could be used toward better understanding human diseases that involve autoimmunity.

In summary, using immunodeficient COL17-humanized mice, we have successfully developed a novel active disease model for BP that continuously produces pathogenic anti-hCOL17 IgG Abs and reproduces the BP phenotype. This study indicates that a humanized animal model is quite valuable not only for analyzing biological function of human molecules but also for investigating pathogenic mechanisms of autoimmune diseases against human proteins. This new BP model can be used for the investigation of underlying mechanisms in the development and progression of BP. Furthermore, it should facilitate the development of novel therapeutic strategies for BP.

Acknowledgments

We thank Professor K. B. Yancey (Department of Dermatology, Medical College of Wisconsin, Milwaukee, WI) for providing the *COL17*$^{m+/+,h+}$ mice, Dr. K. Nishifuji and Professor M. Amagai (Department of Dermatology, Keio University School of Medicine, Tokyo, Japan) for their technical advice and valuable discussions on the ELISPOT assay, Dr. K. Iwabuchi (Division of Immunobiology, Institute for Genetic Medicine, Hokkaido University, Sapporo, Japan) for his valuable discussions, and Ms. N. Ikeda, Ms. Y. Kashima, Ms. M. Tanabe, and Ms. K. Sakai for their technical assistance.

Disclosures

The authors have no financial conflicts of interest.

References

1. Nishie, W., D. Sawamura, M. Goto, K. Ito, A. Shibaki, J. R. McMillan, K. Sakai, H. Nakamura, E. Olasz, K. B. Yancey, et al. 2007. Humanization of autoantigen. *Nat. Med.* 13: 378–383.

2. Taneja, V., and C. S. David. 2001. Lessons from animal models for human autoimmune diseases. *Nat. Immunol.* 2: 781–784.
3. Diaz, L. A., H. Ratrie, III, W. S. Saunders, S. Futamura, H. L. Squiquera, G. J. Anhalt, and G. J. Giudice. 1990. Isolation of a human epidermal cDNA corresponding to the 180-kD autoantigen recognized by bullous pemphigoid and herpes gestationis sera. Immunolocalization of this protein to the hemidesmosome. *J. Clin. Invest.* 86: 1088–1094.
4. Giudice, G. J., D. J. Emery, and L. A. Diaz. 1992. Cloning and primary structural analysis of the bullous pemphigoid autoantigen BP180. *J. Invest. Dermatol.* 99: 243–250.
5. Hopkinson, S. B., K. S. Riddelle, and J. C. Jones. 1992. Cytoplasmic domain of the 180-kD bullous pemphigoid antigen, a hemidesmosomal component: molecular and cell biologic characterization. *J. Invest. Dermatol.* 99: 264–270.
6. Bédane, C., J. R. McMillan, S. D. Balding, P. Bernard, C. Prost, J. M. Bonnetblanc, L. A. Diaz, R. A. Eady, and G. J. Giudice. 1997. Bullous pemphigoid and cicatricial pemphigoid autoantibodies react with ultrastructurally separable epitopes on the BP180 ectodomain: evidence that BP180 spans the lamina lucida. *J. Invest. Dermatol.* 108: 901–907.
7. Ishiko, A., H. Shimizu, A. Kikuchi, T. Ebihara, T. Hashimoto, and T. Nishikawa. 1993. Human autoantibodies against the 230-kD bullous pemphigoid antigen (BPAG1) bind only to the intracellular domain of the hemidesmosome, whereas those against the 180-kD bullous pemphigoid antigen (BPAG2) bind along the plasma membrane of the hemidesmosome in normal human and swine skin. *J. Clin. Invest.* 91: 1608–1615.
8. Zillikens, D., P. A. Rose, S. D. Balding, Z. Liu, M. Olague-Marchan, L. A. Diaz, and G. J. Giudice. 1997. Tight clustering of extracellular BP180 epitopes recognized by bullous pemphigoid autoantibodies. *J. Invest. Dermatol.* 109: 573–579.
9. Giudice, G. J., D. J. Emery, B. D. Zelickson, G. J. Anhalt, Z. Liu, and L. A. Diaz. 1993. Bullous pemphigoid and herpes gestationis autoantibodies recognize a common non-collagenous site on the BP180 ectodomain. *J. Immunol.* 151: 5742–5750.
10. Amagai, M., K. Tsunoda, H. Suzuki, K. Nishifuji, S. Koyasu, and T. Nishikawa. 2000. Use of autoantigen-knockout mice in developing an active autoimmune disease model for pemphigus. *J. Clin. Invest.* 105: 625–631.
11. Olasz, E. B., J. Roh, C. L. Yee, K. Arita, M. Akiyama, H. Shimizu, J. C. Vogel, and K. B. Yancey. 2007. Human bullous pemphigoid antigen 2 transgenic skin elicits specific IgG in wild-type mice. *J. Invest. Dermatol.* 127: 2807–2817.
12. Nelson, K. C., M. Zhao, P. R. Schroeder, N. Li, R. A. Wetsel, L. A. Diaz, and Z. Liu. 2006. Role of different pathways of the complement cascade in experimental bullous pemphigoid. *J. Clin. Invest.* 116: 2892–2900.
13. Nishifuji, K., M. Amagai, M. Kuwana, T. Iwasaki, and T. Nishikawa. 2000. Detection of antigen-specific B cells in patients with pemphigus vulgaris by enzyme-linked immunospot assay: requirement of T cell collaboration for autoantibody production. *J. Invest. Dermatol.* 114: 88–94.
14. Sitaru, C., S. Mihai, C. Otto, M. T. Chiriac, I. Hausser, B. Dotterweich, H. Saito, C. Rose, A. Ishiko, and D. Zillikens. 2005. Induction of dermal-epidermal separation in mice by passive transfer of antibodies specific to type VII collagen. *J. Clin. Invest.* 115: 870–878.
15. Shimizu, H., J. N. McDonald, A. R. Kennedy, and R. A. Eady. 1989. Demonstration of intra- and extracellular localization of bullous pemphigoid antigen using cryofixation and freeze substitution for postembedding immunoelectron microscopy. *Arch. Dermatol. Res.* 281: 443–448.
16. Shimizu, H., A. Ishida-Yamamoto, and R. A. Eady. 1992. The use of silver-enhanced 1-nm gold probes for light and electron microscopic localization of intra- and extracellular antigens in skin. *J. Histochem. Cytochem.* 40: 883–888.
17. Takae, Y., T. Nishikawa, and M. Amagai. 2009. Pemphigus mouse model as a tool to evaluate various immunosuppressive therapies. *Exp. Dermatol.* 18: 252–260.
18. Shibaki, A., A. Sato, J. C. Vogel, F. Miyagawa, and S. I. Katz. 2004. Induction of GVHD-like skin disease by passively transferred $CD8^+$ T-cell receptor transgenic T cells into keratin 14-ovalbumin transgenic mice. *J. Invest. Dermatol.* 123: 109–115.
19. Bianchi, L., S. Gatti, and G. Nini. 1992. Bullous pemphigoid and severe erythrodermic psoriasis: combined low-dose treatment with cyclosporine and systemic steroids. *J. Am. Acad. Dermatol.* 27: 278.
20. Curley, R. K., and C. A. Holden. 1991. Steroid-resistant bullous pemphigoid treated with cyclosporin A. *Clin. Exp. Dermatol.* 16: 68–69.
21. Thivolet, J., H. Barthelemy, G. Rigot-Muller, and A. Bendelac. 1985. Effects of cyclosporin on bullous pemphigoid and pemphigus. *Lancet* 325: 334–335.
22. Barthélémy, H., J. Thivolet, F. Cambazard, A. Bendelac, G. Mauduit, F. Granier, and A. Frappaz. 1986. [Cyclosporin in the treatment of bullous pemphigoid: preliminary study]. *Ann. Dermatol. Venereol.* 113: 309–313.
23. Chen, R., G. Ning, M. L. Zhao, M. G. Fleming, L. A. Diaz, Z. Werb, and Z. Liu. 2001. Mast cells play a key role in neutrophil recruitment in experimental bullous pemphigoid. *J. Clin. Invest.* 108: 1151–1158.
24. Liu, Z., L. A. Diaz, J. L. Troy, A. F. Taylor, D. J. Emery, J. A. Fairley, and G. J. Giudice. 1993. A passive transfer model of the organ-specific autoimmune disease, bullous pemphigoid, using antibodies generated against the hemidesmosomal antigen, BP180. *J. Clin. Invest.* 92: 2480–2488.
25. Liu, Z., G. J. Giudice, S. J. Swartz, J. A. Fairley, G. O. Till, J. L. Troy, and L. A. Diaz. 1995. The role of complement in experimental bullous pemphigoid. *J. Clin. Invest.* 95: 1539–1544.
26. Jordon, R. E., S. Kawana, and K. A. Fritz. 1985. Immunopathologic mechanisms in pemphigus and bullous pemphigoid. *J. Invest. Dermatol.* 85: 72s–78s.
27. Provost, T. T., and T. B. Tomasi, Jr. 1973. Evidence for complement activation via the alternate pathway in skin diseases, I. Herpes gestationis, systemic lupus erythematosus, and bullous pemphigoid. *J. Clin. Invest.* 52: 1779–1787.
28. Sitaru, C., S. Mihai, and D. Zillikens. 2007. The relevance of the IgG subclass of autoantibodies for blister induction in autoimmune bullous skin diseases. *Arch. Dermatol. Res.* 299: 1–8.
29. Aricha, R., T. Feferman, S. Fuchs, and M. C. Souroujon. 2008. Ex vivo generated regulatory T cells modulate experimental autoimmune myasthenia gravis. *J. Immunol.* 180: 2132–2139.
30. Sheng, J. R., L. Li, B. B. Ganesh, C. Vasu, B. S. Prabhakar, and M. N. Meriggioli. 2006. Suppression of experimental autoimmune myasthenia gravis by granulocyte-macrophage colony-stimulating factor is associated with an expansion of $FoxP3^+$ regulatory T cells. *J. Immunol.* 177: 5296–5306.
31. McGeachy, M. J., L. A. Stephens, and S. M. Anderton. 2005. Natural recovery and protection from autoimmune encephalomyelitis: contribution of $CD4^+CD25^+$ regulatory cells within the central nervous system. *J. Immunol.* 175: 3025–3032.
32. O'Connor, R. A., K. H. Malpass, and S. M. Anderton. 2007. The inflamed central nervous system drives the activation and rapid proliferation of $Foxp3^+$ regulatory T cells. *J. Immunol.* 179: 958–966.
33. Kaul, R., M. Shenoy, E. Goluszko, and P. Christadoss. 1994. Major histocompatibility complex class II gene disruption prevents experimental autoimmune myasthenia gravis. *J. Immunol.* 152: 3152–3157.
34. Zhang, G. X., B. G. Xiao, M. Bakhiet, P. van der Meide, H. Wigzell, H. Link, and T. Olsson. 1996. Both $CD4^+$ and $CD8^+$ T cells are essential to induce experimental autoimmune myasthenia gravis. *J. Exp. Med.* 184: 349–356.
35. Aoki-Ota, M., K. Tsunoda, T. Ota, T. Iwasaki, S. Koyasu, M. Amagai, and T. Nishikawa. 2004. A mouse model of pemphigus vulgaris by adoptive transfer of naive splenocytes from desmoglein 3 knockout mice. *Br. J. Dermatol.* 151: 346–354.
36. Christadoss, P., M. Poussin, and C. Deng. 2000. Animal models of myasthenia gravis. *Clin. Immunol.* 94: 75–87.
37. Mendel, I., N. Kerlero de Rosbo, and A. Ben-Nun. 1995. A myelin oligodendrocyte glycoprotein peptide induces typical chronic experimental autoimmune encephalomyelitis in $H\text{-}2^b$ mice: fine specificity and T cell receptor Vβ expression of encephalitogenic T cells. *Eur. J. Immunol.* 25: 1951–1959.
38. Büdinger, L., L. Borradori, C. Yee, R. Eming, S. Ferencik, H. Grosse-Wilde, H. F. Merk, K. Yancey, and M. Hertl. 1998. Identification and characterization of autoreactive T cell responses to bullous pemphigoid antigen 2 in patients and healthy controls. *J. Clin. Invest.* 102: 2082–2089.
39. Lin, M. S., C. L. Fu, G. J. Giudice, M. Olague-Marchan, A. M. Lazaro, P. Stastny, and L. A. Diaz. 2000. Epitopes targeted by bullous pemphigoid T lymphocytes and autoantibodies map to the same sites on the bullous pemphigoid 180 ectodomain. *J. Invest. Dermatol.* 115: 955–961.
40. Thoma-Uszynski, S., W. Uter, S. Schwietzke, G. Schuler, L. Borradori, and M. Hertl. 2006. Autoreactive T and B cells from bullous pemphigoid (BP) patients recognize epitopes clustered in distinct regions of BP180 and BP230. *J. Immunol.* 176: 2015–2023.
41. Delgado, J. C., D. Turbay, E. J. Yunis, J. J. Yunis, E. D. Morton, K. Bhol, R. Norman, C. A. Alper, R. A. Good, and R. Ahmed. 1996. A common major histocompatibility complex class II allele HLA-DQB1* 0301 is present in clinical variants of pemphigoid. *Proc. Natl. Acad. Sci. USA* 93: 8569–8571.
42. Xu, L., N. Robinson, S. D. Miller, and L. S. Chan. 2001. Characterization of BALB/c mice B lymphocyte autoimmune responses to skin basement membrane component type XVII collagen, the target antigen of autoimmune skin disease bullous pemphigoid. *Immunol. Lett.* 77: 105–111.
43. Sitaru, C., M. T. Chiriac, S. Mihai, J. Büning, A. Gebert, A. Ishiko, and D. Zillikens. 2006. Induction of complement-fixing autoantibodies against type VII collagen results in subepidermal blistering in mice. *J. Immunol.* 177: 3461–3468.
44. Ishikawa, F., M. Yasukawa, B. Lyons, S. Yoshida, T. Miyamoto, G. Yoshimoto, T. Watanabe, K. Akashi, L. D. Shultz, and M. Harada. 2005. Development of functional human blood and immune systems in NOD/SCID/IL2 receptor γ $chain^{null}$ mice. *Blood* 106: 1565–1573.
45. Ito, M., H. Hiramatsu, K. Kobayashi, K. Suzue, M. Kawahata, K. Hioki, Y. Ueyama, Y. Koyanagi, K. Sugamura, K. Tsuji, et al. 2002. NOD/SCID/γ_c^{null} mouse: an excellent recipient mouse model for engraftment of human cells. *Blood* 100: 3175–3182.
46. Kumar, P., H. S. Ban, S. S. Kim, H. Wu, T. Pearson, D. L. Greiner, A. Laouar, J. Yao, V. Haridas, K. Habiro, et al. 2008. T cell-specific siRNA delivery suppresses HIV-1 infection in humanized mice. *Cell* 134: 577–586.
47. Yajima, M., K. Imadome, A. Nakagawa, S. Watanabe, K. Terashima, H. Nakamura, M. Ito, N. Shimizu, M. Honda, N. Yamamoto, and S. Fujiwara. 2008. A new humanized mouse model of Epstein-Barr virus infection that reproduces persistent infection, lymphoproliferative disorder, and cell-mediated and humoral immune responses. *J. Infect. Dis.* 198: 673–682.
48. Watanabe, Y., T. Takahashi, A. Okajima, M. Shiokawa, N. Ishii, I. Katano, R. Ito, M. Ito, M. Minegishi, N. Minegishi, et al. 2009. The analysis of the functions of human B and T cells in humanized NOD/shi-scid/γc^{null} (NOG) mice (hu-HSC NOG mice). *Int. Immunol.* 21: 843–858.

Successful Treatment of Nail Lichen Planus with Topical Tacrolimus

Hideyuki Ujiie, Akihiko Shibaki, Masashi Akiyama and Hiroshi Shimizu
Department of Dermatology, Hokkaido University Graduate School of Medicine, North 15 West 7, Kita-ku, Sapporo 060-8638, Japan. E-mail: h-ujiie@med.hokudai.ac.jp
Accepted November 4, 2009.

Sir,

Nail lichen planus (NLP) is characterized by thinning, longitudinal ridging and distal splitting of the nail plate (1, 2). Although mild NLP is usually asymptomatic, deformation of the fingernails is cosmetically distressing. Failure to treat NLP results in nail loss or permanent nail dystrophy in some cases. Therefore the condition should be treated effectively in its early stage. NLP is usually resistant to topical corticosteroid therapy, but successful treatment has been reported with intralesional or systemic administration of corticosteroids (2–4). However, some patients are unable to tolerate the side-effects of systemic corticosteroids.

Topical tacrolimus has been reported as a safe, effective therapy for cutaneous (5, 6), oral (7–9) and vulvar lichen planus (LP) (9–11), even in patients whose lesions have shown recalcitrance to other treatments (7, 10). However, topical tacrolimus treatment for NLP has never been reported. We report here five cases of NLP treated successfully with tacrolimus ointment.

CASE REPORTS

Five Japanese patients with NLP were treated with 0.1% tacrolimus ointment. The mean age of the five patients (4 males and 1 female) was 40.2 years (age range 11–58 years). All of the patients were diagnosed with NLP on the basis of clinical history, typical clinical appearance and histopathological features. No patient had any symptoms suggesting lupus erythematosus or photosensitivity. There was no history of nail matrix trauma, or drug intake that could cause lichenoid drug eruption. All of these cases demonstrated multiple nail lesions on the fingers and/or toes. In one patient, the disease affected all 20 nails. All the fingernails were affected in three other patients, including two cases that presented with additional nail lesions on both big toes. The most common clinical signs were thinning of nails and onycholysis, which were observed in all of the patients. Longitudinal ridging and onychorrhexis were present in four cases. The NLP was not associated with any objective symptom, such as burning, itching or pain, in any of the cases. A 58-year-old patient had concomitant localized reticular oral LP, although no patient had cutaneous, otic or genital lesions at any time during the follow-up. An 11-year-old patient had mild atopic dermatitis; the four adult patients had no other dermatological conditions. The clinical diagnosis was confirmed by histopathological examination in all cases. Biopsy specimens taken from the affected nail matrix demonstrated band-like lymphocyte infiltration in the nail matrix and the nail bed dermis, as well as hyperkeratosis, acanthosis and hypergranulosis of the epidermis, which are histopathological features typically observed in NLP.

The mean duration of the disease prior to the topical tacrolimus treatment was 24 months (range 4–84 months). We followed up all the patients for at least 15 months (mean 39.0 months; range 15–71 months). Four of the patients had been treated with topical corticosteroids, with no or slight improvement, before the tacrolimus therapy. In all the cases, 0.1% topical tacrolimus (Protopic ointment 0.1%, Astellas Pharma Inc., Tokyo, Japan) was administered twice a day on one side of the nail plates and periungual regions of the fingers and/or toes, and a topical corticosteroid (from the classification "very strong" or "strongest") was simultaneously started on the other side for a comparison of relative efficacy. In all cases, the affected nails treated with topical tacrolimus began to improve within 6 months after the initiation of treatment (mean 2.8 months; range 1–6 months), whereas no obvious changes, or only slight improvement, were observed in the nails treated with topical corticosteroids, suggesting that tacrolimus ointment had higher therapeutic efficacy than topical corticosteroids (Fig. 1). All the lesions were then treated uniformly with topical tacrolimus. All of the patients showed marked improvement (Fig. 2). Mild onycholysis and splitting of the nails remained in some of the patients. Reticular oral LP observed in a 58-year-old patient remained after his NLP lesions had improved. Two patients who discontinued topical tacrolimus application showed no exacerbation of their lesions at 16 and 36 months of follow-up, respectively. Two other patients continue to use topical tacrolimus once or twice daily as a supportive treatment, which keeps their lesions stable. The remaining patient stopped visiting our clinic after remission. No adverse effects were noted in any of the cases.

DISCUSSION

Topical corticosteroid therapy is commonly considered as a first-line treatment for NLP, although it is usually ineffective. Oral prednisone and intramuscular triamcinolone acetonide have been reported as effective against NLP (2–4), but prolonged or repeated use of

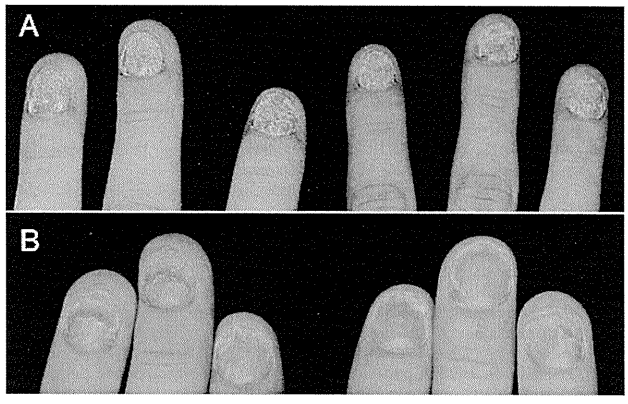

Fig. 1. (A) Nail lichen planus in an 11-year-old male patient before treatment. The fingernails show very severe thinning. The right-hand fingernails were treated with topical tacrolimus and the left-hand ones with diflucortolone valerate ointment twice daily (comparative application). (B) The same patient after 5 months of comparative application. Significant clinical improvement of the right-hand fingernails (*right*) was noted compared with the left-hand ones (*left*).

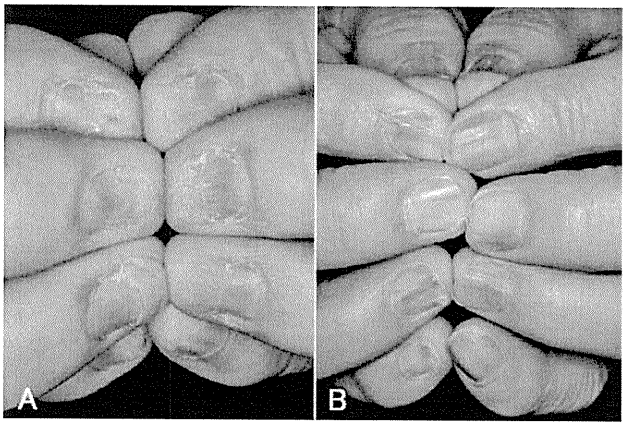

Fig. 2. (A) Nail lichen planus in a 58-year-old male patient. The fingernails show severe distal thinning and onycholysis before treatment. (B) Significant improvement after 18 months of topical tacrolimus treatment.

systemic corticosteroids may cause considerable side-effects.

Tacrolimus is a macrolide immune modulator that produces strong immunosuppression by inhibiting T-cell activation. It interacts with a cyclophilin-like cytoplasmic protein, FK506 binding protein, and this complex interferes with the phosphatase activity of calcineurin, resulting in the inhibition of proinflammatory cytokine genes transcription. Because activated T cells are likely to play a central role in the pathogenesis of LP (1, 12, 13), topical tacrolimus has been tried for the treatment of LP. Previous studies have reported that topical tacrolimus is effective for 88–100% of cases of oral LP (7–9) and 94% of cases of vulvar LP (10). Based on these data, we speculated that topical tacrolimus could also be effective against NLP. In this study, all five cases with NLP responded fairly well to topical tacrolimus, even though 4 had intractable lesions that had shown resistance to topical corticosteroids. Comparative study of the efficacy of topical tacrolimus and topical corticosteroids revealed that topical tacrolimus was more effective than topical corticosteroids in all of the cases.

Recent studies demonstrated that nail dystrophy associated with chronic paronychia (14) and eczema (15) improved with topical tacrolimus, which suggests that topical tacrolimus could penetrate the periungual skin enough to improve the nail dystrophy. In addition, the remarkable thinning of the nails and onychorrhexis seen in most of our NLP cases make it possible that the tacrolimus ointment penetrated the damaged nail plates.

The majority of oral LP and vulvar LP cases respond to topical tacrolimus within one month (7–11), whereas the present NLP patients required several months to start to regress (mean 2.8 months).

At present, two out of the five patients have been continuing once- or twice-daily application for 35 and 63 months, respectively, to keep their lesions under control. Two other patients have been stable without topical tacrolimus for more than one year. However, we should be aware of the possibility that NLP can recur, because previous reports have mentioned that oral or vulvar LP lesions usually returned after withdrawal of topical tacrolimus (7, 10). Further analysis with longer follow-up is required to confirm the long-term prognosis of NLP after the cessation of topical tacrolimus therapy.

The authors declare no conflict of interest.

REFERENCES

1. Boyd AS, Neldner KH. Lichen planus. J Am Acad Dermatol 1991; 25: 593–619.
2. Tosti A, Peluso AM, Fanti PA, Piraccini BM. Nail lichen planus: clinical and pathologic study of twenty-four patients. J Am Acad Dermatol 1993; 28: 724–730.
3. Evans AV, Roest MA, Fletcher CL, Lister R, Hay RJ. Isolated lichen planus of the toe nails treated with oral prednisolone. Clin Exp Dermatol 2001; 26: 412–414.
4. Tosti A, Piraccini BM, Cambiaghi S, Jorizzo M. Nail lichen planus in children: clinical features, response to treatment, and long-term follow-up. Arch Dermatol 2001; 137: 1027–1032.
5. Al-Khenaizan S, Al Mubarak L. Ulcerative lichen planus of the sole: excellent response to topical tacrolimus. Int J Dermatol 2008; 47: 626–628.
6. Fortina AB, Giulioni E, Tonin E. Topical tacrolimus in the treatment of lichen planus in a child. Pediatr Dermatol 2008; 25: 570–571.
7. Byrd JA, Davis MD, Bruce AJ, Drage LA, Rogers RS, 3rd. Response of oral lichen planus to topical tacrolimus in 37 patients. Arch Dermatol 2004; 140: 1508–1512.
8. Olivier V, Lacour JP, Mousnier A, Garraffo R, Monteil RA, Ortonne JP. Treatment of chronic erosive oral lichen planus with low concentrations of topical tacrolimus: an open prospective study. Arch Dermatol 2002; 138: 1335–1338.
9. Vente C, Reich K, Rupprecht R, Neumann C. Erosive mucosal lichen planus: response to topical treatment with tacrolimus. Br J Dermatol 1999; 140: 338–342.
10. Byrd JA, Davis MD, Rogers RS, 3rd. Recalcitrant symptomatic vulvar lichen planus: response to topical tacrolimus. Arch Dermatol 2004; 140: 715–720.
11. Kirtschig G, Van Der Meulen AJ, Ion Lipan JW, Stoof TJ. Successful treatment of erosive vulvovaginal lichen planus with topical tacrolimus. Br J Dermatol 2002; 147: 625–626.
12. Shiohara T, Moriya N, Nagashima M. The lichenoid tissue reaction. A new concept of pathogenesis. Int J Dermatol 1988; 27: 365–374.
13. Shiohara T, Nickoloff BJ, Moriya N, Gotoh C, Nagashima M. In vivo effects of interferon-gamma and anti-interferon-gamma antibody on the experimentally induced lichenoid tissue reaction. Br J Dermatol 1988; 119: 199–206.
14. Rigopoulos D, Gregoriou S, Belyayeva E, Larios G, Kontochristopoulos G, Katsambas A. Efficacy and safety of tacrolimus ointment 0.1% vs. betamethasone 17-valerate 0.1% in the treatment of chronic paronychia: an unblinded randomized study. Br J Dermatol 2009; 160: 858–860.
15. Lee DY, Kim WS, Lee KJ, Kim JA, Park JH, Cho HJ, et al. Tacrolimus ointment in onychodystrophy associated with eczema. J Eur Acad Dermatol Venereol 2007; 21: 1137–1138.

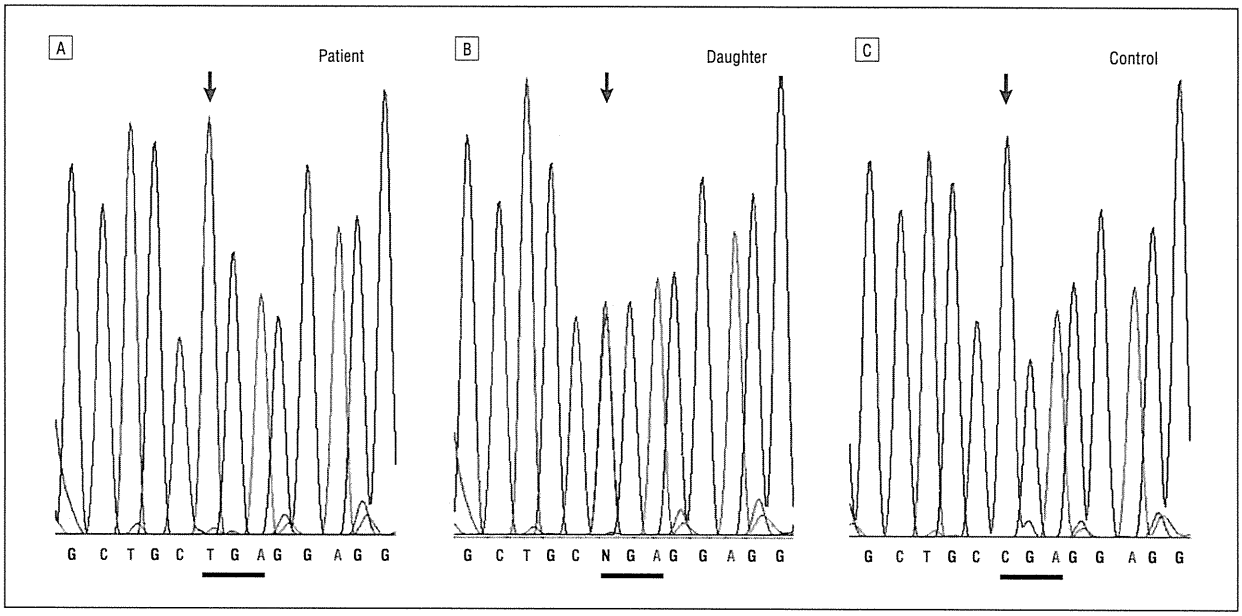

Figure 2. Sequence analysis of the *TAP2* gene. Detection of the mutation from genomic DNA was performed by polymerase chain reaction amplification of *TAP2* exon 3 for the patient (A) (mutant homozygous), a daughter (B) (heterozygous), and a healthy control (C) (native sequence).

previously ulcerated lesions of the right leg (Figure 1D and E), and the limb was amputated. The neoplasia recurred and metastasized, and the patient died.

Blood samples were obtained from the proband and relatives, and lymphocyte subpopulations were analyzed by flow cytometry. The numbers of NK cells, γδ T lymphocytes, and $CD8^+$ αβ T cells as well as the CD4/CD8 ratios were found to be normal and comparable to those found in controls and her relatives. The HLA I expression in the patient's lymphocytes was severely reduced (30 times lower than in healthy controls). The HLA serologic typing in the patient was unsuccessful. We extracted RNA from peripheral blood mononuclear cells; all coding exons of *TAP1* and *TAP2* genes (OMIM 170260 and 170261, respectively) were amplified by reverse transcriptase–PCR, and further sequencing analysis was performed. A previously unreported *TAP2* missense mutation was detected. The patient was homozygous for a C→T transition at nucleotide 628 (*TAP2* exon 3) (**Figure 2**), leading to a premature stop at codon 210 between the fifth and the sixth transmembrane domains of *TAP2*. Her mother and daughters were heterozygous for the mutated allele. In addition, high-resolution molecular HLA typing demonstrated that the patient was homozygous for the haplotype HLA-A*0301, Cw*1701, B*5001, DRB1*0301, DQA*0501/DQB1*0201, and DPB1*0401.

Comment. We report herein an SCC originating in a chronic ulcer of a patient with type I BLS and a novel *TAP2* gene mutation. Abnormal expression of HLA class I has been reported in many human neoplasias,[5] including skin cancer. Our findings suggest that TAP-impaired HLA class I expression could influence the course of SCC originating in chronic ulcers and could be related to escape from cytotoxic T-lymphocyte surveillance during disease progression.

Agustín España, MD
Cecilia González-Santesteban, PhD
Laura Martínez-Martínez, PhD
Ana Bauzá, MD
Oscar de la Calle-Martín, PhD

Correspondence: Dr España, Department of Dermatology, University Clinic of Navarra, School of Medicine, University of Navarra, PO Box 4209, Pamplona, Navarra, Spain (aespana@unav.es).
Financial Disclosure: None reported.

1. de la Salle H, Hanau D, Fricker D, et al. Homozygous human TAP peptide transporter mutation in HLA class I deficiency. *Science.* 1994;265(5169):237-241.
2. Moins-Teisserenc HT, Gadola SD, Cella M, et al. Association of a syndrome resembling Wegener's granulomatosis with low surface expression of HLA class I-molecules. *Lancet.* 1999;354(9190):1598-1603.
3. Peaper DR, Cresswell P. Regulation of MHC class I assembly and peptide binding. *Annu Rev Cell Dev Biol.* 2008;24:343-368.
4. Zimmer J, Andres E, Donato L, Hanau D, Hentges F, de la Salle H. Clinical and immunological aspects of HLA class I deficiency. *QJM.* 2005;98(10):719-727.
5. Garrido F, Ruiz-Cabello F, Cabrera T, et al. Implications for immunosurveillance of altered HLA class I phenotypes in human tumours. *Immunol Today.* 1997;18(2):89-95.

Hereditary Benign Telangiectasia: Two Families With Punctate Telangiectasias Surrounded by Anemic Halos

Hereditary benign telangiectasia (HBT), one of the primary telangiectatic disorders, is characterized by various patterns of widespread cutaneous telangiectasias.[1,2] It is distinguished from hereditary hemorrhagic telangiectasia by the absence of recurrent bleeding and systemic involvement. Herein we describe

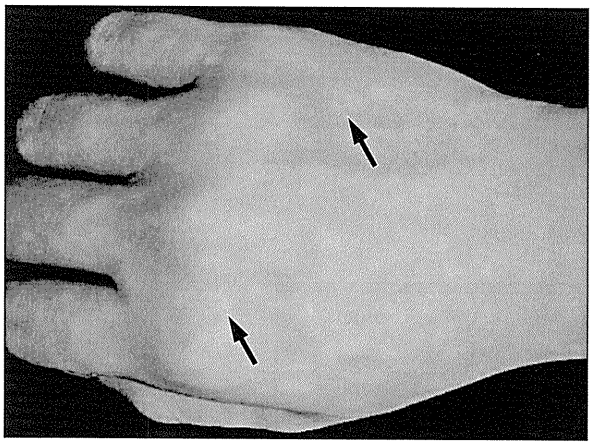

Figure 1. Skin lesions seen on the proband of family 1 with hereditary benign telangiectasia. Multiple punctate telangiectasias surrounded by anemic halos (arrows) are visible on the dorsal surface of the right hand.

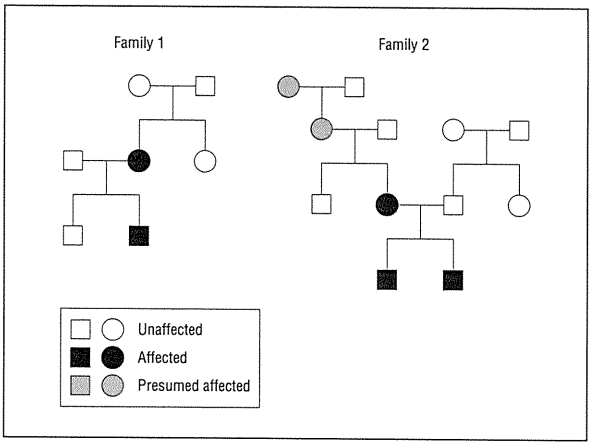

Figure 2. Pedigrees of the 2 families with hereditary benign telangiectasia showing punctate telangiectasias surrounded by anemic halos. Circles indicate female family members; squares, male family members.

2 families with HBT that show unique fine telangiectasias surrounded by anemic halos.

Report of Cases. *Case 1.* A 16-year-old boy was seen for asymptomatic telangiectasias with halos that had appeared several months earlier with no preceding episodes. Physical examination revealed multiple fine telangiectasias surrounded by pale macules as large as 5 mm on the dorsal surfaces of the hands (**Figure 1**), the radial aspects of the forearms and thighs, and on the trunk. The pale macules disappeared during application of mechanical pressure, which indicated that they were anemic halos. He also had numerous fine telangiectasias on the lips and irregularly shaped telangiectatic macules on the chest, right arm, and right thigh. His mother had similar fine telangiectasias surrounded by anemic halos on the right forearm (**Figure 2**). Laboratory data of the proband showed no abnormalities in blood cell count, liver function, renal function, or blood coagulation time. Skin specimens obtained from a telangiectasia with an anemic halo on the dorsal surface of the proband's hand demonstrated no specific changes. All of the telangiectatic lesions persisted for more than 5 years.

Case 2. A 14-year-old boy was referred for evaluation of asymptomatic fine telangiectasias surrounded by halos that had been noticed several weeks earlier without any preceding episodes. Multiple punctate telangiectasias surrounded by anemic halos were seen on the dorsal surfaces of the hands and on the radial aspects of the forearms. He had some irregularly shaped telangiectatic macules on the face, trunk, and extremities.

His mother had macular telangiectasias on her back and face, and his 11-year-old brother had similar lesions on his left hand and upper extremities (Figure 2). None of the family members had remarkable medical histories or hemorrhagic episodes. His maternal grandmother and great-grandmother seemed to have some reddish macular lesions, but the details were unclear (Figure 2).

No specific abnormalities were detected in laboratory examinations of the proband. Histologic and ultrastructural examinations of the biopsy specimens from the proband demonstrated no specific changes. To date, the cutaneous lesions of the proband remain unchanged for over 5 years.

Comment. Initially described in 1971,[2] HBT is probably an autosomal dominant disorder.[1] Various patterns of telangiectatic lesions, including plaquelike, radiating, arborizing, reticulated, mottled, spiderlike, and punctate, have been described in HBT.[1,2] Punctate telangiectasias surrounded by anemic halos have rarely been reported.[3] The mechanism whereby the anemic halo develops remains unclear. In eruptive pseudoangiomatosis, a rare skin disorder characterized by acute angiomalike papules or macules, the surrounding halo might be due to vasoconstriction around the vasodilatation of the papular angiomatous lesions.[4] In nevus anemicus, the anemic macule is thought to be caused by increased local vascular reactivity to catecholamines.[5] The findings from the families described herein indicate that punctate telangiectasias surrounded by anemic halos should be recognized as unique and characteristic features of HBT.

Hideyuki Ujiie, MD
Kazuo Kodama, MD, PhD
Masashi Akiyama, MD, PhD
Hiroshi Shimizu, MD, PhD

Correspondence: Dr Ujiie, Department of Dermatology, Hokkaido University Graduate School of Medicine, N15 W7, Kita-ku, Sapporo 060-8638, Japan (h-ujiie@med.hokudai.ac.jp).
Financial Disclosure: None reported.
Additional Contributions: Kokichi Hamasaka, MD, provided helpful information on the cases.

1. Brancati F, Valente EM, Tadini G, et al. Autosomal dominant hereditary benign telangiectasia maps to the CMC1 locus for capillary malformation on chromosome 5q14. *J Med Genet.* 2003;40(11):849-853.
2. Ryan TJ, Wells RS. Hereditary benign telangiectasia. *Trans St Johns Hosp Dermatol Soc.* 1971;57(1):148-156.
3. Puppin D Jr, Rybojad M, Morel P. Hereditary benign telangiectasia: two case reports. *J Dermatol.* 1992;19(6):384-386.
4. Neri I, Patrizi A, Guerrini V, Ricci G, Cevenini R. Eruptive pseudoangiomatosis. *Br J Dermatol.* 2000;143(2):435-438.
5. Greaves MW, Birkett D, Johnson C. Nevus anemicus: a unique catecholamine-dependent nevus. *Arch Dermatol.* 1970;102(2):172-176.

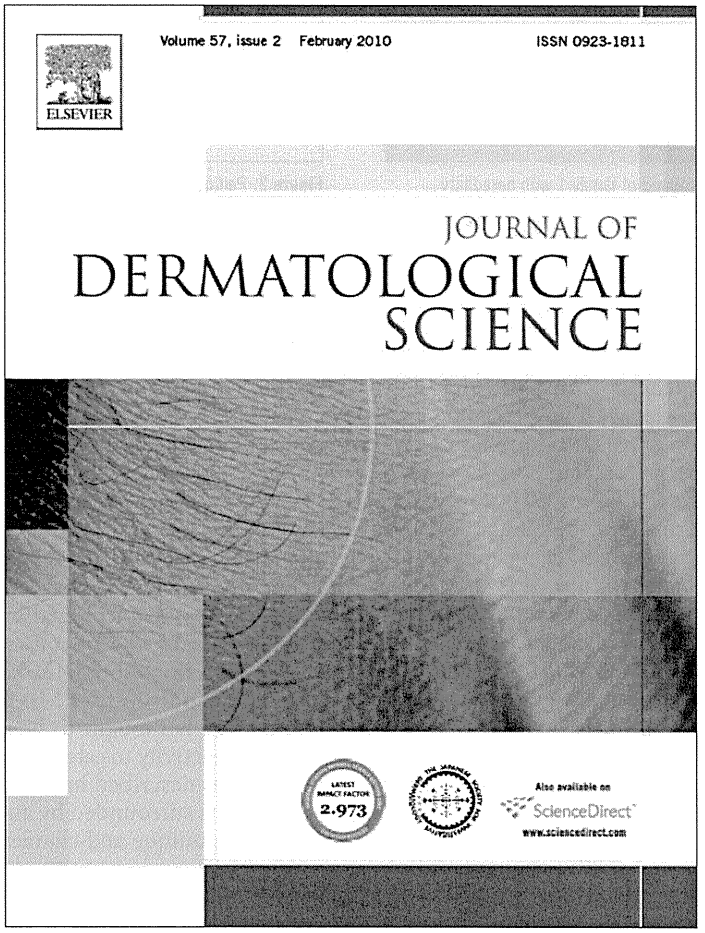

Journal of Dermatological Science 57 (2010) 102–107

Contents lists available at ScienceDirect

Journal of Dermatological Science

journal homepage: www.elsevier.com/jds

Epidermal triglyceride levels are correlated with severity of ichthyosis in Dorfman–Chanarin syndrome

Mayumi Ujihara [a], Kimiko Nakajima [a], Mayuko Yamamoto [a], Mika Teraishi [a], Yoshikazu Uchida [b], Masashi Akiyama [c], Hiroshi Shimizu [c], Shigetoshi Sano [a,*]

[a] Department of Dermatology, Kochi Medical School, Kochi University, Oko-cho, Nankoku, Japan
[b] Department of Dermatology, School of Medicine, University of California San Francisco, CA, USA
[c] Department of Dermatology, Hokkaido University Graduate School of Medicine, Sapporo, Japan

ARTICLE INFO

Article history:
Received 17 July 2009
Received in revised form 28 October 2009
Accepted 29 October 2009

Keywords:
Dorfman–Chanarin syndrome
Neutral lipid storage disease with ichthyosis
Triglycerides
CGI-58

ABSTRACT

Background: Dorfman–Chanarin syndrome (DCS), also referred to as neutral lipid storage disease with ichthyosis, is a rare autosomal recessive form of nonbullous congenital ichthyosiform erythroderma, characterized by the presence of intracellular lipid droplets in multiorgans. DCS patients often have mutations in CGI-58, which is an activator of adipose triglyceride lipase (ATGL), leading to accumulation of triglycerides (TG).
Objective: To study whether a patient with DCS demonstrates TG accumulation in the epidermis and to analyze whether TG levels are correlated with skin disease activity.
Methods: Skin specimen from a 62-year-old man with DCS was stained with oil red O, and analyzed on electromicrographs. Sequencing analysis of *CGI-58* was performed using the patient's blood cells. The scales from the lesion were subject to lipid analysis by high-performance thin-layer chromatography (HPTLC).
Results: The patient demonstrated ichthyoform erythroderma with a distinct seasonal fluctuation: his skin lesions were aggravated in summer but resolved during winter. Epidermis of the lesion showed intracellular lipid droplets. Sequencing analysis revealed a novel missense mutation in the exon 3 of *CGI-58* gene. Lipid analysis of the scales from his lesions, compared with those from normal human control, revealed increased levels of triglycerides (TG) but, in turn, decreased levels of free fatty acids, suggesting dysfunction of adipose TG lipase. Notably, the TG levels in the scales from the patient were positively correlated with the severity of ichthyosis.
Conclusion: These results suggest that TG accumulation by epidermal keratinocytes directly contributes to ichthyosiform phenotype of DCS.

1. Introduction

Dorfman–Chanarin syndrome (DCS, MIM275630), also referred to as neutral lipid storage disease with ichthyosis (NLSDI), is a rare autosomal recessive disorder, in which an excess of triacylglycerols (TG) accumulates in various cells [1–3]. DCS is characterized by nonbullous congenital ichthyosiform erythroderma associated with the presence of cytoplasmic neutral lipid droplets in keratinocytes, as well as a variety of cells in the body including peripheral leukocytes (Jordans' anomaly) [4] and liver cells [5]. Therefore, extracutaneous manifestations of DCS include hepatomegaly (fatty liver), myopathy, cataract, sensoryneural deafness and other neurological symptoms. While cutaneous manifestation of DCS represented nonbullous congenital ichthyosiform erythroderma of mild to moderate severity, the clinical heterogeneity is present. For example, they included nonspecific ichthyosiform dermatosis with alopecia [5], sparing of the face [6], or even no erythematous change [7]. In addition, a case with DCS exhibited ichthyotic erythematous plaques, which frequently migrated as a clinical feature resembling erythrokeratoderma variabilis [8].

Mutations in *CGI-58* gene, which is also called *ABHD5* and encodes a member of α/β-hydrolase family of proteins, have been identified as a cause of DCS [9]. CGI-58 is an activator of adipose triglyceride lipase (ATGL) contributing to TG lipolysis [10,11], which depends on its association with perilipin [12]. CGI-58 mutations, therefore, abrogated lipolysis and induced a systemic accumulation of lipids droplets. *CGI-58* gene is located on 3p21, encoding seven exons, and expressed in many tissues including

* Corresponding author. Tel.: +81 88880 2363; fax: +81 88880 2364.
E-mail address: sano.derma@kochi-u.ac.jp (S. Sano).

0923-1811/$36.00
doi:10.1016/j.jdermsci.2009.10.016

skin [9,13]. In patients with DCS, *CGI-58* mutations were associated with defective formation of lamellar granules [14]. Lipid micro-inclusions in lamellar granules formed a non-lamellar phase within the stratum corneum interstices, contributing to permeability barrier dysfunction characterized by ichthyosis in DCS [15]. To date, 16 mutations of *CGI-58* gene have been reported [16], and each of mutations affected the structure of CGI-58, leading to dysfunction of the downstream lipase ATGL. The mutations found in DCS include missense mutations, nonsense mutations, splice site mutations, a deletion or insertion in exons causing a frameshift and premature termination of translation [9,14]. For instance, forced expression of mutant *CGI-58* gene into an adipocyte cell line resulted in its inability to interact with perilipin, leading to mistargeting of CGI-58 to the lipid droplets [12]. Further, expression of functional CGI-58 in DCS fibroblasts restores lipolysis and reversed the abnormal TG accumulation [10].

Mutations in the gene encoding ATGL (*PNPLA2*) have been identified as the cause of neutral lipid storage disease with myopathy (NLSDM) [17]. NLSDM patients and ATGL-deficient mice exhibited DCS-like features associated with TG accumulation in multiple tissues including adipose tissue, muscle, heart and other organs, however, devoid of ichthyosis [18,17].

Therefore, the mutations in *CGI-58* gene result in development of ichthyosis in addition to abnormalities shared with NLSDM. This notion indicated that CGI-58 possessed an additional function required for lipid metabolism in the epidermis [17]. Previous studies demonstrated that the ultrastructure of DCS included abnormal lipid micro-inclusions within lamellar bodies and resulting lamellar/non-lamellar phase separation or clefts in the intercellular spaces of cornified layer [3,14,15]. Very recent study revealed that CGI-58 expression was increased during differentiation and localized in lamellar granules of keratinocytes and likely to be involved in barrier formation [13]. Given that TG is the content of lipid deposition in DCS, unsolved question is that the ultrastructural aberrancy in the epidermis is similar to other inherited, lipid storage diseases associated with ichthyosis, such as Refsum disease, Sjögren–Larsson syndrome [15]. Thus, no direct evidence has been shown regarding the link of TG deposition in the epidermis and ichthyosiform phenotype found in DCS.

In the present study, we demonstrate a DCS patient with a novel mutation of *CGI-58* gene in one allele, showing an abrupt, seasonal variation of ichthyosiform lesions. Biochemical study of his scales revealed the increased levels of TG, which was positively correlated with severity of ichthyosis.

2. Materials and methods

2.1. Patient

This study was approved by the Institute Ethical Review Board of the Kochi Medical School, Kochi University, and performed according to the Declaration of Helsinki Principles. Skin samples and scales were provided from a patient with DCS (see Section 3 for further details) and healthy donors with sunburn as controls.

2.2. Electron microscopic examination

The skin biopsy specimens were fixed with 2% glutaraldehyde in 0.1 M sodium cacodylate (pH 7.3) for 2 h at room temperature. The skin samples were post-fixed for 1 h at room temperature with 2% osmium tetroxide in 0.1 M cacodylate buffer. The samples were then dehydrated in a graded series of ethanol. Following dehydration, the samples were transferred to propylene oxide and embedded in Epon 812 (TAAB Laboratories Equipment, Berkshire, England). They were observed with a Hitachi H-7100 electron microscope (Hitachi High-Technologies, Tokyo, Japan).

2.3. Determination of TEWL and water holding capability

To assess basal permeability barrier function, we used a Tewameter (TEWAMETER TM300, Courage and Khazaka, Cologne, Germany) over six separate sites. Water holding capability was determined using a corneometer (CORNEOMETER CM825, Courage and Khazaka) over six separate sites.

2.4. Mutation analysis

The method for mutation detection of *CGI-58* gene was performed as previously reported [9]. Briefly, genomic DNA isolated from peripheral blood was subject to PCR amplification, followed by direct automated sequencing. Oligonucleotide primers used for amplification of all exons 1–7 of *CGI-58* gene and detailed PCR conditions were described elsewhere [14,9].

2.5. Lipid analysis of scales

Total lipids were extracted from scales as described previously [19]. Scales from sunburn in a healthy individual were used as control for this assay, since we confirmed that its lipid content did not significantly differ from that previously reported from non-sunburn scales in normal donors. The individual lipid species were separated by high-performance thin-layer chromatography (HPTLC), followed by quantification by scanning densitometry as described previously with the following solvent systems: (1) benzene–n-hexane (1:1) to 8.5 cm; and n-hexane–diethyl ether–acetic acid (70:30:1, v/v/v) to 5 cm. Lipids were visualized after treatment with cupric acetate–phosphoric acid, and heating to 160 °C for 15 min. The quantity of each lipid was determined by spectrodensitometry, as previously described [19].

3. Results

3.1. Case presentation

A 62-year-old Japanese man visited our hospital in October 2006 complaining of slightly pruritic, dry skin with scaling. From early childhood the patient had been suffering from scaly skin lesions over the entire body, which were characterized by a seasonal variation with a marked aggravation in summer. He was the first and an only child from non-consanguineous parents. There was no family history of congenital ichthyosis or abnormal lipid diseases. The patient was mildly obese with a BMI 26.5 (height: 157 cm, weight: 65 kg). His skin was dry and mildly erythrodermic with fine scales, surrounding normal-looking skin with irregular patterns on the trunk, lateral side of upper arms, the right scapular region, bilateral breasts, and buttocks (Fig. 1a and b). The skin of the dorsa of the hands was shiny with prominent creases and lamellar scaling was in lower legs (Fig. 1c). There were spiny keratoses on his palms, but the nails, teeth and hair appeared normal.

Transepidermal water loss (TEWL) and skin hydration were assessed in the involved skin and normal-looking, uninvolved skin of the upper arm. TEWL of the ichthyosiform lesion (18.0 g h^{-1} m^{-2}) was within the normal range (0–10, very good; 10–15, good; 15–20, fair; 25–30, poor; more than 30, very poor) but slightly higher than uninvolved skin (14.5 g h^{-1} m^{-2}). On the other hand, the water retention capability was markedly impaired in the lesion (6.7, normal >60) compared with the uninvolved skin (63.8). These results indicated that the ichthyosiform lesions of this patient showed an intact permeability barrier but a markedly decreased hydration, which was contrast to a previous study showing abnormal barrier function [15].

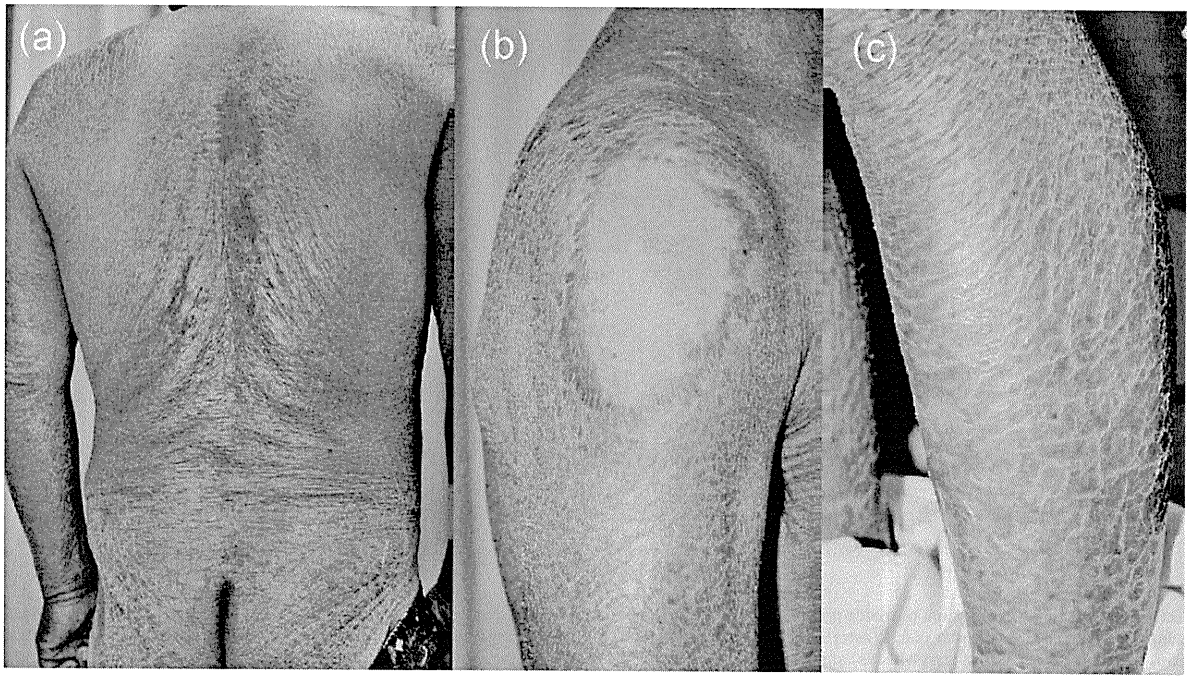

Fig. 1. Clinical appearance. (a) Scaly ichthyosiform erythroderma. (b) Sharply demarcated site of uninvolved skin on the lateral aspect of the upper arm. (c) Large, membranous scales on the legs.

Laboratory investigation revealed abnormalities of hepatic enzymes including aspartate aminotransferase 85 IU L^{-1} (normal range: 10–35), alanine aminotransferase 79 IU L^{-1} (5–40), γ-glutamyltransferase 497 IU L^{-1} (5–70), and alkaline phosphatase 366 IU L^{-1} (100–344). The computed tomography and ultrasonic examination demonstrated hepatic hypertrophy and fatty liver. Steroid sulfatase activity in the peripheral blood sample was normal. Although white blood cell count was normal, there were distinct intracytoplasmic vacuoles in polynuclear leukocytes (Fig. 2c) and monocytes (Fig. 2d), which were presumed to be Jordan's anomaly [4]. No evidence of muscle weakness or neurological abnormality was obtained.

3.2. Histologic features and lipid droplets in the epidermis

Skin biopsy specimen from the right thigh revealed hyperkeratosis and mild acanthosis but the granular layer was normal (Fig. 2a). There were mild mononuclear cell infiltrates around blood vessels in the dermis. Groups and strands of fat cells were found embedded among the proliferating collagen bundles of the

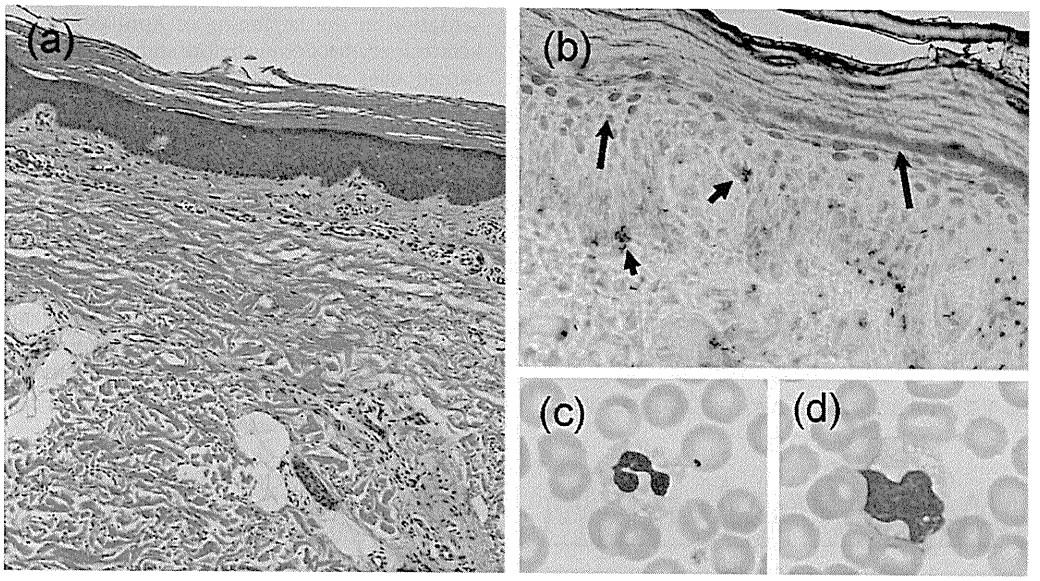

Fig. 2. Histologic appearance and lipid deposition in epidermis and white blood cells. (a) H&E staining of formalin-fixed, paraffin-embedded lesional skin section from the patient's left thigh. Hyperkeratosis, acanthosis and mild perivascular infiltrates are noted (40×). (b) Oil red O staining of frozen section (200×). The cornified and granular layers are strongly stained with oil red O (arrows), which also stained cells of basal layer in punctate (arrowheads). Intracytoplasmic vacuoles within peripheral blood neutrophils (c, 1000×) and monocytes (d, 1000×) represent Jordan's anomaly.

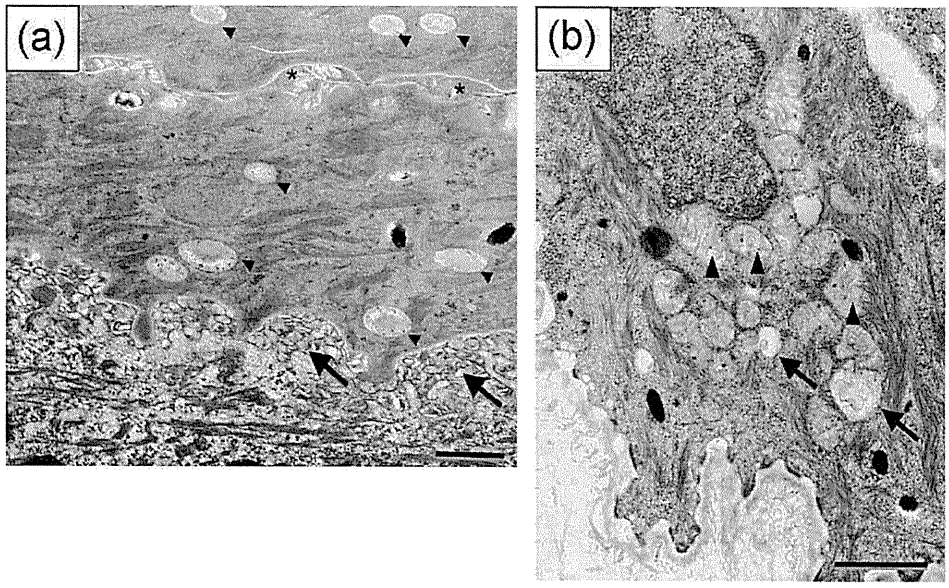

Fig. 3. Electron micrographs after osmium tetroxide post-fixation and Epon embedding. (a) Electron-lucent vacuoles are present within corneocytes (arrowheads). There are amorphous materials in the intracellular spaces (asterisks). Abnormal lamellar granules are aggregated in the stratum granulosum/stratum corneum interface (arrows). Scale bar, 0.5 μm. (b) Giant mitochondria (arrowheads) and lucent vacuoles (arrows) are seen in the cytoplasm of basal cells. Scale bar, 1 μm.

dermis (Fig. 2a). Staining with oil red O demonstrated lipid droplets within keratinocytes in the stratum granulosum, the stratum corneum (Fig. 2b, arrows) and the basal layer (Fig. 2b, arrowheads). Taken together, we diagnosed him as DCS.

3.3. Ultrastructural findings

Electron microscopic examination of the lesional skin of the patient revealed a number of electron-lucent vacuoles, presumably lipid droplets, within the cytoplasm of corneocytes and deposits of amorphous materials in the intercellular spaces (Fig. 3a). Accumulation of abnormal lamellar granules lacking the normal lamellar content was also seen in the stratum granulosum/stratum corneum interface (arrows in Fig. 3a). These features were consistent with previous studies with DCS [14,15]. Furthermore, giant mitochondria and lucent vacuoles were found within the basal keratinocytes (Fig. 3b), suggesting an abnormal lipid metabolism of keratinocytes as previously described [20].

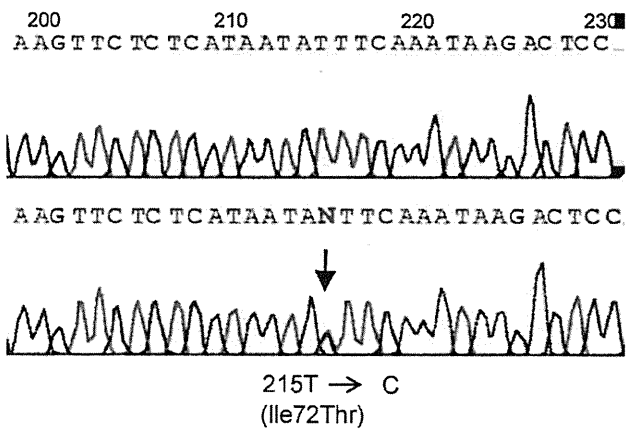

Fig. 4. Sequencing analysis of *CGI-58* gene. A novel heterozygous 215T>C transition in the exon 3, that substitutes isoleucine for threonine at position 72 (I72T).

3.4. Mutation in CGI-58 gene

Mutation analysis of *CGI-58* gene of the patient's blood revealed a heterozygous point mutation (215T>C) in the exon 3 (Fig. 4). This novel mutation substituted isoleucine for threonine at position 72 (Ile72Thr), indicating a missense mutation. However, further analysis of another allele failed to detect any other pathogenic mutation within the all seven exons and exon–intron borders of this gene (data not shown).

3.5. Seasonal variation of disease activity

Notably, his skin lesions were aggravated in summer. As shown in Fig. 5, the ichthyosiform lesions recurred with some irritant sensation in the beginning of April every year, and developed keratotic erythrodermia before summer. The ichthyosiform lesions spread over entire body, but several areas were spared, for example, around nipples. This manifestation was very similar to a previous report, in which a patient with DCS showed erythematous migratory patches resembling erythrokeratoderma variabilis [8]. With lowering the air temperature in autumn, the ichthyosiform plaques were remitted, and mostly, if any, disappeared by mid-winter. Interestingly, his skin lesions showed some resolution when he stayed away from hot temperature even in the mid-summer, but were immediately aggregated when stayed outside. This suggested that the development of the ichthyosiform change was dependent on environmental temperature. Such feature was also similar to the aforementioned DCS patient [8].

3.6. Lipid analysis of scales

Scales were collected from the involved sites of the patient at aggravation and remission stages. Scales from a non-ichthyotic individual with sunburn dermatitis were used as a control. Although there was no difference in the quantity of cholesterol between the patient and control, triglycerides (TG) were increased by two- and threefold over control in the scales at remission and aggravation stage, respectively (Fig. 6). Thus, TG levels in scales were correlated with the severity of ichthyotic condition. In